KeAi

CHINESE ROOTS
GLOBAL IMPACT

#### Contents lists available at ScienceDirect

# Petroleum Science





# Original Paper

# Reconstruction of the thermal evolution since the late paleozoic in the Ounan Sag, Eastern Qaidam Basin, NW China: New constraints from vitrinite reflectance data and (U—Th)/He thermochronology



Chang Zhong <sup>a, b, c</sup>, Hui Shi <sup>a, b, c</sup>, Xiao-Yin Tang <sup>a, b, c, \*</sup>, Hao Zhang <sup>a, b, c, \*\*</sup>, Yuan-Yuan Yang <sup>a, b, c</sup>, Jun-Jie Hu <sup>a, b, c</sup>, Xiao-Jie Wei <sup>a, b, c</sup>, Jia-Qi Wang <sup>d</sup>

- <sup>a</sup> Institute of Geomechanics, Chinese Academy of Geological Sciences, Beijing, 100081, China
- <sup>b</sup> Key Laboratory of Paleomagnetism and Tectonic Reconstruction, Ministry of Natural Resources, Beijing, 100081, China
- <sup>c</sup> Key Laboratory of Petroleum Geomechanics, China Geological Survey, Beijing, 100081, China
- <sup>d</sup> SinoProbe Center, Chinese Academy of Geological Sciences, Beijing, 100037, China

#### ARTICLE INFO

# Article history: Received 17 October 2023 Received in revised form 24 February 2024 Accepted 16 May 2024 Available online 18 May 2024

Edited by Jie Hao and Meng-Jiao Zhou

Keywords:
Thermal evolution
Eastern Qaidam Basin
Late Paleozoic
Apatite and zircon (U—Th)/He
thermochronology
Vitrinite reflectance

#### ABSTRACT

Reconstructing the thermal evolution of the eastern Qaidam Basin is important for gaining a deeper understanding of its lithospheric geodynamics and for more accurate hydrocarbon evaluation and prediction. This article presents a set of new apatite and zircon (U-Th)/He thermochronological ages. Combined with 336 vitrinite reflectance  $(R_0)$  data, the thermal history of the Ouanan Sag in the eastern Qaidam Basin has been reconstructed using inversion models. Three detrital samples from the Ounan Sag shows that the apatite (U—Th)/He ages are primarily concentrated in the range of 17.0 Ma to 76.5 Ma and that the zircon (U-Th)/He ages range from 200 Ma to 289.3 Ma. The time-temperature models demonstrate that the Ounan Sag experienced rapid subsidence and heating from the Carboniferous to late Permian, and exhumation/cooling events from the end of Permian to the Triassic. This thermal evolution was influenced by the widespread intrusion of plutons, and the collision and orogenesis caused by asthenosphere upwelling below the Qaidam arc, and slab rollback of the Southern Kunlun oceanic lithosphere, respectively. Additionally, our models depict the main exhumation/cooling stages since the Paleogene and a reheating event in the Miocene as a result of the intensifying growth of the Oinghai -Tibet Plateau and local sedimentary loading, followed by the initial India-Eurasia collision. Furthermore, the eastern Qaidam Basin experienced consistent heating during the late Paleozoic, reaching the maximum paleotemperature and geothermal gradient in the late Permian, with values of ~230 °C and ~43-44 °C/km, respectively. This study suggests that the source rocks in the most upper member of upper Carboniferous Keluke  $(C_2k)$  Formations in the Ounan Sag reached the gas generation stage in the

© 2024 The Authors. Publishing services by Elsevier B.V. on behalf of KeAi Communications Co. Ltd. This is an open access article under the CC BY license (http://creativecommons.org/licenses/by/4.0/).

### 1. Introduction

The study of thermal evolution of sedimentary basins provides important parameters for understanding geodynamics and tectonic evolution and insight into hydrocarbon generation and

accumulation (Quinlan et al., 1993; Qiu et al., 2011; Chang et al., 2018; Zhu et al., 2018; Yang et al., 2022, 2023). It can be reconstructed by the thermal indicator, such as vitrinite reflectance ( $R_0$ ), fission track, and (U—Th)/He dating (Qiu et al., 2022). The Qaidam Basin is a significant tectonic unit in the northern Qinghai—Tibet Plateau and was involved in the Cenozoic growth of this plateau, which was related to the indentation of India into Asia starting at approximately 65—50 Ma (Meyer et al., 1998; Tapponnier et al., 2001; Yin et al., 2002; Zuza et al., 2017). The basin is situated at the junction of the Bayanhar Terrane and the North China Craton, and is surrounded by the Tarim Craton to the west (Song et al., 2017; Zuza and Yin, 2017; Dong et al., 2021; Sun et al., 2022)

<sup>\*</sup> Corresponding author. Institute of Geomechanics, Chinese Academy of Geological Sciences, Beijing, 100081, China.

<sup>\*\*</sup> Corresponding author. Institute of Geomechanics, Chinese Academy of Geological Sciences, Beijing, 100081, China.

E-mail addresses: tangxiaoyin@mail.cgs.gov.cn (X.-Y. Tang), zhhao@cags.ac.cn (H. Zhang).

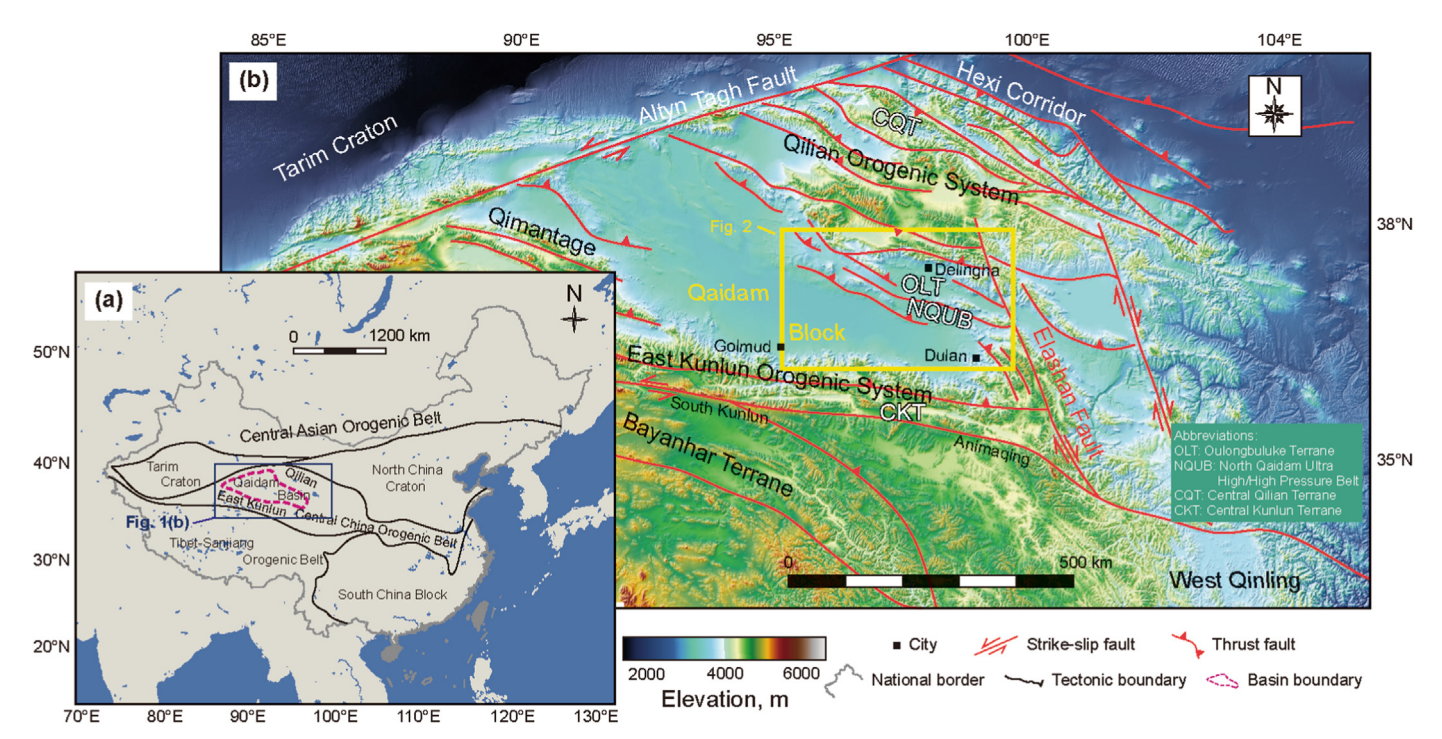


Fig. 1. Schematic tectonic map of (a) mainland China and (b) the Qilian-Qaidam-East Kunlun collage show main blocks, terranes and orogens (Zhao and Cawood, 2012; Sun et al., 2022)

(Fig. 1). In addition, the basin has occupied a pivotal position in the Tethyan tectonic domain since the late Paleozoic and has unique characteristics of lithospheric geodynamics and tectono-thermal evolution (Li, 2006; Metcalfe, 2013; Wu et al., 2016; Zuza et al., 2017). It is suggested that the Kunlun-Qaidam arc was structurally juxtaposed with the Bayanhar Terrane during the final closure of the Tethyan oceanic realm (Sun et al., 2022). In response to this collisional orogenesis, a few researchers believed that the rapid exhumation/cooling event took place in the basin-surrounding orogenic systems, which was indicated by the 40Ar/39Ar thermochronological data (Peng, 2015). Furthermore, the early Cenozoic exhumation events in the eastern Qaidam Basin are also consistent with the initial growth of the Qinghai-Tibet Plateau (Clark et al., 2010). However, there are only a few quantitative studies on the timing and magnitude of the exhumation/cooling events that occurred in the shallow crust of the eastern Qaidam Basin with insufficient thermal indicators in the western Ounan Sag (Liu et al., 2020b), which is unfavorable for further understanding the deep lithospheric process of the Kunlun-Qaidam arc and Qinghai-Tibet Plateau.

Recently, advances in drillings within the lower Paleozoic in the Ounan Sag, eastern Qaidam Basin, have led to discoveries of hydrocarbon resources, indicating a promising outlook for further petroliferous exploration (Ma et al., 2012; Liu et al., 2012, 2020a; Li et al., 2019; Peng et al., 2021; Shi et al., 2022, 2023a, 2023b). The upper Carboniferous Keluke ( $C_2k$ ) Formations with thick dark shale have been recognized as potential hydrocarbon source rocks and a promising reservoir. Hydrocarbons are predominantly high-quality light oil and wet gas (Shi et al., 2023a, 2023b). The vitrinite reflectance of the C<sub>2</sub>k source rocks in the eastern Ounan Sag ranges between ~1.5% and 1.6%, indicating that the organic matter has generally evolved into a high maturity stage (Shi et al., 2022, 2023a, 2023b). However, the evolution of hydrocarbon maturation for the Carboniferous strata has been poorly constrained. This is attributed to the conflicting study of the timing constraints on paleotemperature evolution for the Carboniferous strata in the eastern Qaidam

Basin. On the one hand, a few researchers believe that the Carboniferous strata reached their maximum paleotemperature in the Cenozoic time, which was indicated by the mega-burial of ca. 4000 m (Ma et al., 2012; Li et al., 2017). On the other hand, some studies have reported higher paleotemperature than that in the late Mesozoic to Cenozoic. The C2k Formations in the Ounan Sag, eastern Qaidam Basin exceeded the paleotemperature of 180  $^{\circ}\text{C}$  in the mid-late Permian (e.g., Liu et al., 2012, 2020a; Guo et al., 2022). This has been attributed to the consistent thermal fluctuations from ca. 290-210 Ma (Wu et al., 2016; Cheng et al., 2017; Sun et al., 2022). These fluctuations are also indicated by detrital zircon ages, pointing to the formation and flare-up of plutons (e.g., Gehrels et al., 2003; Guo et al., 2009; Chen et al., 2015; Cheng et al., 2017; Sun et al., 2022) compared with magmatic stasis since the Late Jurassic (e.g., Cheng et al., 2019). Therefore, it is crucial to quantitatively reconstruct the thermal history since the late Paleozoic time for more accurate hydrocarbon evaluation and prediction in the eastern Qaidam Basin.

In this study, the initial temperature models generated from  $R_0$  data are constructed. We present a set of new thermochronological ages and conduct time–temperature modeling constrained by the apatite and zircon (U—Th)/He ages. In addition, we reconstruct the burial-thermal models of an outcrop section and three wells. These models are used to reconstruct the thermal evolution in the Ounan Sag and to discuss the tectonic factors controlling the exhumation/cooling history and the potential genesis of the heating process since the late Paleozoic in the eastern Qaidam Basin. Finally, we analyze the implications for hydrocarbon generation.

# 2. Geological settings

### 2.1. Tectonic evolution

The Qaidam Basin is surrounded by the Qilian accretionary zones to the north, the East Kunlun orogenic systems, Bayanhar Terrane to the south, and the Tarim Craton to the west. It is a

component of the Central China orogenic system (Song et al., 2017; Zuza and Yin, 2017; Sun et al., 2022) (Fig. 1(a), (b)). The tectonic architecture of the Qaidam Basin is governed by a collage of crustal fragments with rigid Precambrian crystalline basement, including the Central Kunlun, Qaidam, Oulongbuluke, and Central Qilian microblocks from south to north (Xiao et al., 2009; Song et al., 2017; Dong et al., 2021). These tectonic units fused and experienced a prolonged subduction history related to the South Kunlun Ocean, a major branch of the Paleo-Tethys Ocean, whose closure led to the formation of Pangea from the late Paleozoic to early Mesozoic (Metcalfe, 2013; Zhao et al., 2018; Sun et al., 2022). After the violent Devonian orogenesis, the deposits forming in the Qaidam Basin transitioned into Carboniferous marine deposits during the continuous transgression related to the expansion of the Zongwulong rift zone in the north (Pan et al., 2012; Sun et al., 2019, Sun et al., 2022). At the end of the Carboniferous, sporadic volcanic eruptions occurred (ca. 294 Ma) (Liu and Qian, 2023; Zhou et al., 2023; Zhong et al., 2024b), and massive amounts of intermediate-silicic to mafic magma and arc-related intrusions formed in the ring-shaped Eastern Kunlun arc until the Late Triassic (Chen et al., 2015; Cheng et al., 2017; Li et al., 2022). In response to collisional orogenesis, intense forebulge flexural elevation and orogen unroofing took place in the broad Kunlun-Qaidam arc (Li et al., 2017; Sun et al., 2022).

The Qaidam Basin is truncated by the left-lateral strike-slip Altyn Tagh Fault to the west (Fig. 1(a)), which links eastward with NE-SW-striking structures extending toward Mongolia (Darby et al., 2005). The northern basin consists of several subparallel NW-SE-to WNW-ESE-trending ranges that have developed in association with folds, thrusts, and/or strike-slip faults accommodating the northward motion of the Tibetan Plateau since the late Mesozoic (Meyer et al., 1998; Yin et al., 2002). The Qaidam Basin and its surrounding orogenic systems have undergone multiple phases of deformation since the Mesozoic and accommodated considerable crustal thickening during the Cenozoic in response to the India-Asia collision and post-collisional convergence (Meyer et al., 1998; Meng and Fang, 2008; Yin et al., 2008; Cheng et al., 2019, 2021). Notably, a lack of magmatism and post-collisional extensional/transtensional tectonic settings during the early to mid-Jurassic has been recognized in the Qilian Shan-northern Qaidam Basin region and is inferred to be a result of far-field effects of subduction processes along the southern margins of the continent (Yin and Harrison, 2000; Cheng et al., 2017; Cheng et al., 2019).

# 3. Stratigraphy and sedimentology

The study area mainly comprises three depositional sags with two uplifts, including the Ounan Sag/Uplift, Delingha Sag, Huobuxun Sag, and Emnic Uplift (Fig. 2), which are controlled by three major faults. The eastern Qaidam Basin preserves the carbonate-clastic mixed stratigraphic sequence of the Paleozoic (e.g., Sun et al., 2016; Wei et al., 2021). The sedimentary strata overlying the basement consist of the lower Carboniferous Chengqianggou  $(C_1ch)$  and Huaitoutala  $(C_1h)$  Formations and the upper Carboniferous Keluke  $(C_2k)$  and Zhabusagaxiu  $(C_2zh)$  Formations (QBMR, 1991). In the Ounan Sag, early Carboniferous sedimentation was dominated by (bioclastic) micrite mudstone deposition, while the late Carboniferous was characterized by frequent deposition of interbedded limestone, sandstone, and coal (Sun et al., 2016; Wei et al., 2018, 2021). At the end of the Carboniferous, the basin transitioned due to transgression, leading to the formation of an epicontinental clastic-carbonate sequence and combinations of sluice reservoirs and cover rocks (Ma et al., 2020; Shi et al., 2022, 2023a, 2023b). The East Kunlun and Qilian

Orogenic Systems are dominated by marine limestone with clastic intervals. Among these units, the Zongwulong Group comprises a set of slightly metamorphosed black shales that are intercalated with limestones, intermediate volcanic interlayers, cherts, and pillow lavas (QBGMR, 1991), and the Permian Nuoyinhe Group is dominated by thick, massive, fossiliferous limestone with thin clastic and acidic volcanic intervals mostly at the base (QBGMR, 1991). The middle Permian to Triassic rocks in the Eastern Kunlun are dominated by continental arc granite (ca. 270–240 Ma) with interbedded siltstone and intermediate—felsic volcanics (e.g., Li et al., 2022).

Starting in the Late Triassic, deposition in the eastern Qaidam Basin has been dominated by continental fill (Peng, 2015; Liu et al., 2020b). The basin preserves scattered lacustrine—fluvial facies deposits, dominated by suites of conglomerate, interbedded sandy mudstone to sandstone, interbedded coal, and even anemoarenite from the Jurassic to Cretaceous (Fig. 3) (Cheng et al., 2019; Hu et al., 2020a; Xiong et al., 2024). Additionally, Cenozoic strata are widely distributed throughout the basin, with their main deposition center systematically located at the geometric center of the basin (Meng and Fang, 2008; Pang et al., 2019; Cheng et al., 2021).

In the Ounan Sag, the Carboniferous strata exhibit the development of diverse hydrocarbon source rocks, comprising three distinct lithological types: dark mud/shale, coal, and mudstone (Duan et al., 2006; Cao et al., 2009; Liu et al., 2020a, 2020b; Shi et al., 2023a, 2023b). Organic geochemical analyses reveal a prevailing humic nature (Type III) in the organic matter of the Carboniferous source rocks, indicating an overall maturity spectrum that spans from mature to highly mature stages (Shi et al., 2022, 2023a. 2023b). The primary hydrocarbon source rocks within the Carboniferous strata are located in the Upper Carboniferous  $C_2k$ Formations. Characterized by an overall burial depth of less than 4500 m, the C2k Formations consist of dark mud/shale with a thickness ranging from approximately 20 m-200 m. The total organic carbon content (TOC) displays variability within the range of 0.28%–21.16% (average 2.3%). Hydrocarbon generation potential  $(S_1+S_2)$  ranges from 0.01 mg/g to 2.44 mg/g (mean 0.35 mg/g), and the chloroform extractable bitumen "A" value is distributed between 0.0017% and 0.0866% (mean 0.0075%) (Duan et al., 2006; Cao et al., 2009; Liu et al., 2020a; Shi et al., 2022, 2023a, 2023b). So far, owing to its conducive conditions for hydrocarbon generation, the C<sub>2</sub>k Formations have been recognized as potential hydrocarbon source rocks and a promising reservoir for shale gas (Liu et al., 2020a; Shi et al., 2022, 2023a, 2023b).

# 4. Methods and data

# 4.1. Vitrinite reflectance $(R_0)$ analyses

Vitrinite reflectance ( $R_0$ ) is a prevalent technique for recovering the thermal history of sedimentary basins, and it has been effectively used to calculate the maximum paleotemperature and simulate the geothermal gradient history and thermal evolution of source rocks (Barker and Goldstein, 1990; Tang et al., 2014; Li et al., 2017; Chang et al., 2018; Hackley, 2020; Kuang et al., 2022).

We collected a total of 336  $R_0$  datasets in the Qaidam Basin (Fig. 4); 194 data points were obtained from source rocks in the Jurassic strata, while 142 data points originated from the Carboniferous strata. One of these datasets has not been published (QDC1, C1h), whereas the remaining data were cited from previous studies (Yu et al., 2000; Duan et al., 2006; Liu et al., 2007; Liu et al., 2020b; Xu et al., 2008; Cao et al., 2009; Chen and Zhang, 2011; Fang et al., 2012; Fu et al., 2014; Li et al., 2017; Dang, 2019; Shi et al., 2022). All  $R_0$  datasets were subjected to conversion with empirical Eq. (1) (Barker and Pawlewicz, 1986):

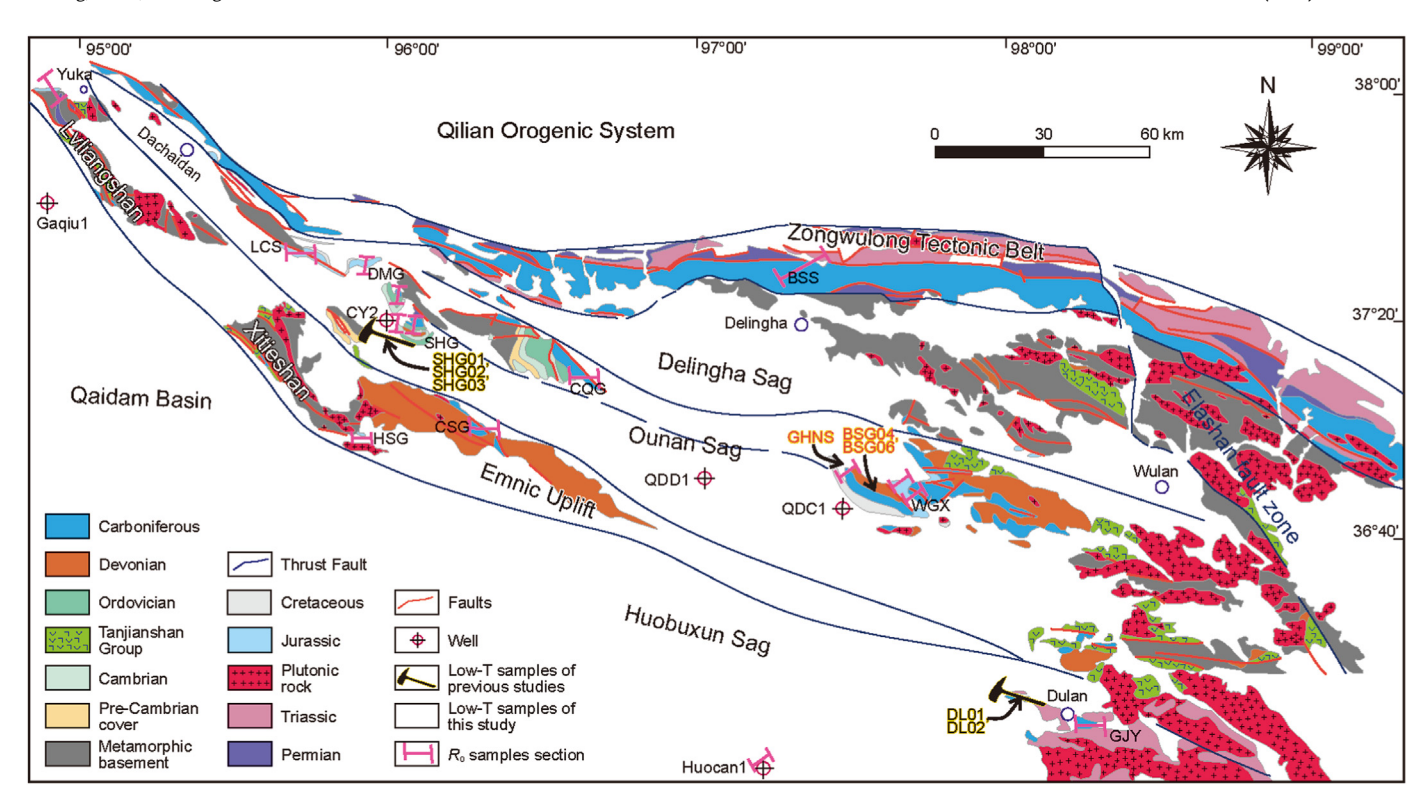


Fig. 2. Simplified geological map of the eastern Qaidam Basin and its surrounding orogenic systems (modified from Sun et al., 2022). The tectonic divisions, distribution of main outcrops, boreholes/wells, and samples were compiled for discussion in the main text. The position of the study area is labeled in Fig. 1(b).

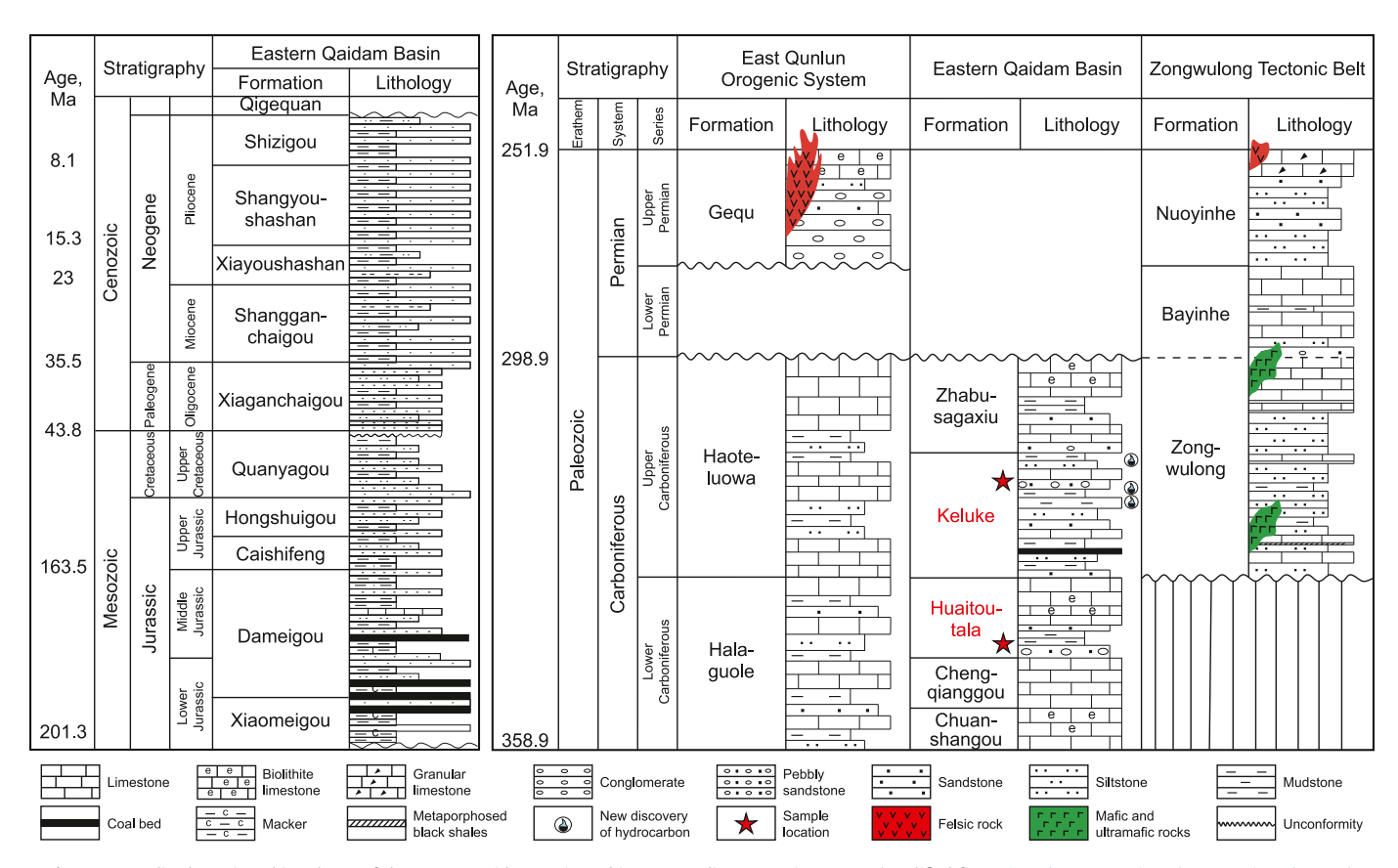
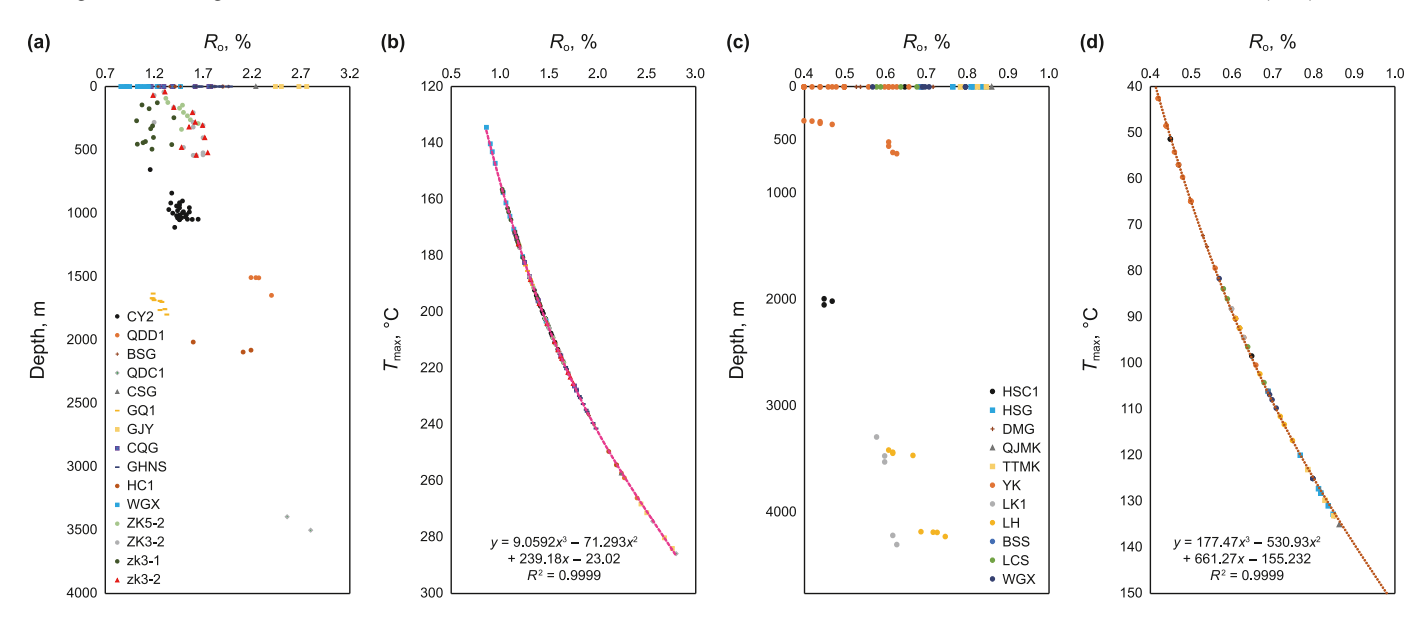


Fig. 3. Generalized stratigraphic column of the eastern Qaidam Basin and its surrounding orogenic systems (modified from Li et al., 2017; Wei et al., 2021; Li et al., 2022).



**Fig. 4.**  $R_0$  datasets in the Qaidam Basin: Single  $R_0$  value versus burial depth (a) and  $T_{\text{max}}$  (b) for the Carboniferous source rocks; Single  $R_0$  value versus burial depth (c) and  $T_{\text{max}}$  (d) for the Jurassic source rocks.

$$ln(R_0) = 0.0078T_{\text{max}} - 1.2, \tag{1}$$

where  $R_0$  refers to vitrinite reflectance, %, and  $T_{\rm max}$  refers to the maximum paleotemperature, °C.

# 4.2. Low-temperature detrital apatite and zircon (U-Th)/He thermochronological (AHe and ZHe) analyses

Low-temperature thermochronology has been extensively used to reconstruct the thermal histories of sedimentary basins (e.g., Qiu et al., 2014; Chang et al., 2017, 2021, 2022; Jiang et al., 2021; Gusmeo et al., 2022; Xu et al., 2023). In recent years, (U-Th)/He thermochronology has become a novel approach for better understanding geological timing (e.g., Reiners et al., 2003; Rohrmann et al., 2012), landscape evolution (e.g., Emmel et al., 2014; Mackintosh et al., 2017; Eizenhöfer et al., 2021, 2023), sedimentary provenance and tectono-thermal evolution (e.g., Gong et al., 2007; Tang et al., 2014, 2019, 2023; Chang et al., 2018, 2019; Pang et al., 2019; Ye et al., 2022). In this study, we synthesized the closure temperature ranges of multiple thermochronological methods; closure temperature ranges represent the temperature-sensitive ranges within which most annealing or He diffusion occurs. Specifically, we employed the AHe and ZHe techniques, with partial retention zones of 30-90 °C and 130-210 °C, respectively (Flowers et al., 2009; Guenthner et al., 2013).

We analyzed three detrital samples from outcrops in the Ounan Sag, eastern Qaidam Basin (Fig. 2 and Table 1). All samples were collected from outcrops in the eastern Ounan Sag and analyzed using both apatite and zircon (U—Th)/He thermochronology. Sample BSG04 and GHNS were collected from the  $C_1h$  Formation, and BSG06 was taken from the bottom of the  $C_2k$  Formation; these samples were all pebbly sandstones. Additionally, we collected 5 data points from the published literature (Liu et al., 2020b); 3 data points (SHG01, SHG02, SHG03) were obtained from a well (CY2) in the western Ounan Sag, and other 2 data points (DL01, DL02) were from outcrops in the eastern area of the eastern Qaidam Basin, relatively close to the eastern Ounan Sag (Fig. 2, Table 1). All data were sourced from the  $C_2k$  Formation (sandstones) and analyzed using zircon (U—Th)/He thermochronology.

Apatite and zircon grains from each sample were selected and separated using conventional heavy liquid and magnetic separation techniques at Hebei Langfang Chengxin Rock Detection Co. Ltd. Subsequently, AHe and ZHe measurements were conducted in the (U—Th)/He Laboratory of the Department of Earth and Environmental Sciences, Dalhousie University, Canada. Three to five acceptable single apatite/zircon grains were obtained from each sample (Table 2 and Table 3). The detailed analytical processes and instrumental conditions of the laboratory have been described in Landry et al. (2016).

# 4.3. Thermal history modeling

To investigate the thermal history of the eastern Qaidam Basin, we modeled the AHe and ZHe thermochronological data using HeFTy software (Ketcham et al., 2007). The HeFTy approach uses constrained Monte Carlo simulations and accounts for the effects of grain size, radiation damage, and cooling rate on the thermal history (Ketcham, 2005; Flowers et al., 2009). The diffusion model proposed by Flowers et al. (2009) was applied to apatite (U-Th)/He dates, while that of Guenthner et al. (2013) was applied to zircon (U-Th)/He dates. We modeled the thermal history for all three samples and incorporated the AHe and ZHe data of the same sample derived from the eastern Ounan Sag (BSG04, BSG06, GHNS). Notably, in addition to considering the temperature data generated from vitrinite reflectance, we integrated both AHe and ZHe data from each sample into one inversion model. Compared with inverting single-type thermochronological data, this combination approach provides more accurate limits on the model due to the combination of two different partial retention systems, resulting in a longer, comparable, and complex thermal history. Regarding the addition of a single grain for thermal modeling, ages that fall outside the expected date range, whether older or younger, would not be suitable for the thermal model inversion. To alleviate the impact of <sup>4</sup>He loss, we chose the single grain with the maximum grain width or moderately older age from each sample for the thermal modeling.

The modeling parameters included uranium, thorium, and samarium for each sample. The initial modeling time was set to be the time when each sample was deposited in the Ounan Sag

**Table 1**The information of (U—Th)/He thermochronological samples collected from the eastern Qaidam Basin.

Sample	Latitude N	Longitude E	Stratigraphic	Lithology	Weighted mean ag	Weighted mean age, Ma			
					AHe	ZHe			
BSG04 <sup>a</sup>	36°53′39″	97°39′27″	C <sub>1</sub> h	Pebbly sandstone	51.87 ± 0.18	252.16 ± 1.11 Ma			
BSG06 <sup>a</sup>	36°53′13″	97°39′27″	$C_2k$	Pebbly sandstone	$41.5 \pm 0.16$	279.67 ± 1.18 Ma			
GHNS <sup>a</sup>	36°57′16″	97°28′55″	$C_1h$	Pebbly sandstone	$38.8 \pm 0.16$	251.07 ± 1.17 Ma			
SHG01 <sup>b</sup>	37°25′06″	96°04′25″	$C_2k$	sandstone	_	$275.2 \pm 35.8 \mathrm{Ma}$			
SHG02 <sup>b</sup>	37°25′06″	96°04′25″	$C_2k$	sandstone	_	$264.8 \pm 35.8 \mathrm{Ma}$			
SHG03 <sup>b</sup>	37°25′06″	96°04′25″	$C_2k$	sandstone	_	275.2 ± 35.8 Ma			
DL01 <sup>b</sup>	36°21′93″	97°54′40″	$C_2k$	sandstone	_	$258.9 \pm 38.4 \mathrm{Ma}$			
DL02 <sup>b</sup>	36°21′93″	97°54′40″	$C_2k$	sandstone	-	$225.4 \pm 33.4 \mathrm{Ma}$			

<sup>&</sup>lt;sup>a</sup> Samples for thermal modeling.

**Table 2**Measured apatite (U—Th)/He data of the Ounan Sag.

Sample	Grain	Corr age, Ma	err., Ma	U, ppm	Th, ppm	147Sm, ppm	e [U] <sup>a</sup>	Th/U	He, nmol/g	Mass, μg	Ft <sup>b</sup>	ESR <sup>c</sup>	Raw age, Ma	err., Ma
BSG04	1	73.7	0.26	20.0	76.3	161.6	38.3	3.82	10.9	3.11	0.70	51.66	51.24	0.26
	2	46.1	0.16	21.1	75.4	86.1	38.9	3.57	6.8	2.90	0.69	50.38	31.76	0.16
	3	35.8	0.13	23.5	56.2	87.3	36.8	2.40	4.8	2.35	0.67	46.26	23.89	0.13
	4	17.0	0.07	6.4	143.5	211.2	40.4	22.58	2.4	1.74	0.62	41.52	10.58	0.07
BSG06	1	28.2	0.12	32.0	33.8	98.3	40.3	1.06	4.6	4.91	0.74	59.70	20.94	0.12
	2	51.5	0.19	14.1	40.1	163.4	24.2	2.85	5.3	6.40	0.76	66.24	39.13	0.19
	3	44.8	0.16	10.9	47.2	105.2	22.3	4.31	4.0	3.76	0.71	55.54	32.00	0.16
GHNS	1	20.9	0.08	23.0	27.0	34.3	29.4	1.18	2.1	1.38	0.62	38.97	12.96	0.08
	2	19.0	0.07	13.6	44.4	245.6	25.0	3.27	1.8	2.54	0.66	46.11	12.64	0.07
	3	76.5	0.32	52.0	51.7	195.2	64.9	0.99	17.2	1.49	0.63	39.99	48.27	0.32

an Effective uranium concentration (U+0.235 Th ppm).

**Table 3**Measured zircon (U—Th)/He data of the Ounan Sag.

Sample	Grain	Corr age, Ma	err., Ma	U, ppm	Th, ppm	147Sm, ppm	e [U] <sup>a</sup>	Th/U	He, nmol/g	Mass, ug	Ft <sup>b</sup>	ESR <sup>c</sup>	Raw age, Ma	err., Ma
BSG04	1	209.7	0.88	180.5	167.9	19.9	219.2	0.93	187.9	4.35	0.74	46.46	156.16	0.88
	2	289.3	1.29	172.6	92.4	4.0	193.9	0.54	241.4	7.09	0.78	53.88	225.80	1.29
	3	257.5	1.16	132.6	60.8	4.8	146.6	0.46	163.9	9.00	0.79	55.96	203.14	1.16
BSG06	1	282.8	1.21	273.1	207.0	3.1	320.8	0.76	387.3	5.82	0.77	52.73	218.92	1.21
	2	274.1	1.21	214.7	124.9	8.2	243.4	0.58	274.6	4.33	0.75	46.39	204.90	1.21
	3	200.0	0.85	50.1	42.9	5.4	60.0	0.86	50.4	5.24	0.77	50.88	153.17	0.85
	4	282.1	1.12	52.5	68.5	22.9	68.4	1.31	83.8	7.49	0.79	56.89	221.85	1.12
GHNS	1	197.0	0.89	292.0	130.6	10.7	322.2	0.45	267.4	5.85	0.77	50.85	151.59	0.89
	2	226.7	1.07	212.8	49.8	3.4	224.3	0.23	224.5	10.16	0.80	59.92	182.37	1.07
	3	257.4	1.18	281.2	106.9	9.6	305.9	0.38	337.5	6.38	0.78	53.18	200.65	1.18
	4	269.1	1.26	305.6	89.7	3.6	326.2	0.29	383.2	7.55	0.79	56.60	213.41	1.26
	5	205.7	0.89	72.0	53.5	0.6	84.4	0.74	75.3	7.52	0.79	57.19	162.62	0.89

<sup>&</sup>lt;sup>a</sup> Effective uranium concentration (U+0.235 Th ppm).

(~350—320 Ma), and the initial surface temperature was 25 °C (Li et al., 2017; Zhang, 2017; Liu et al., 2020b). In addition, before modeling, the programs required four constrained time–temperature intervals. Based on ZHe weighted mean ages (Table 1), and unconformities underlying the lower Jurassic Formations (Liu et al., 2020b; Wang et al., 2022), an initial constraint for all samples was chosen around the late Permian to the early Triassic, with the temperature of 130—210 °C. The Cenozoic constraint was mainly set to the early Paleocene to the late Eocene, as the most AHe weighted mean ages shown around 38—52 Ma, with a temperature of 30—90 °C. In addition, another two constraints were set based on the onset time of sedimentation (around the late Triassic to the early Jurassic) and the stratigraphic unconformity (around the midlate Cretaceous) (QBGMR, 1978) in the eastern Qaidam Basin (Cheng et al., 2019; Hu et al., 2020a; Wang et al., 2020). The

temperature of sedimentation was set to  $20-80\,^{\circ}\text{C}$ , representing the environmental transition from the intermontane to lacustrine conditions (Cheng et al., 2019). The temperature for cooling events was constrained to  $60-120\,^{\circ}\text{C}$ , as the AFT thermal modeling shown in the previous literature (Wang et al., 2022). In addition, we set the thermal modeling to run until 100 good fits were reached for all samples.

# 4.4. Basin modeling

Currently, in the upstream sector, basin modeling aids in the prediction of hydrocarbon occurrence, migration, accumulation, etc., and it incorporates a broad spectrum of geological information (e.g., Hsu and Robinson, 2017; Ashrafi et al., 2020). In this study, one-dimensional (1-D) basin modeling was used to reconstruct the

<sup>&</sup>lt;sup>b</sup> Previously reported samples cited from Liu et al., 2020b.

<sup>&</sup>lt;sup>b</sup> Ft is the a-ejection correction after Farley. (2002).

<sup>&</sup>lt;sup>c</sup> ESR is Grain width, μm.

<sup>&</sup>lt;sup>b</sup> Ft is the a-ejection correction after Farley. (2002).

 $<sup>^{\</sup>text{c}}\,$  ESR is Grain width,  $\mu m.$ 

thermal-burial histories of an outcrop section and three wells (QDD1, QDC1, and CY2) using BasinMod 1D (version 5.4) based on the Easy %R<sub>0</sub> model (Sweeney and Burnham, 1990). We first rebuilt the sedimentary-burial history of the outcrop section (GHNS) and wells based on the strata thickness and drilling data, and then the erosion thicknesses, measured  $R_0$  data, and present-day heat flow values were input as the constraints. The erosion thicknesses in multiple stages were derived from previous studies by OBGMR (1987), Li et al. (2019), Liu et al. (2020b) and Wang et al. (2022). The present heat flow was set to 53.1 mW/m<sup>2</sup> (Zhang, 2017), and the paleo-surface temperature was calculated based on the latitude of the eastern Qaidam Basin using the SWIT model (Wygrala, 1989). Secondly, the paleo-geothermal gradient evolution paths were repeatedly modified as forward modeling for comparing the modeled  $R_0$  paths with the measured  $R_0$  data. When the modeled  $R_0$ paths are consistent with the measured  $R_0$  data (Fig. 5), the geothermal gradient path at this time is considered to be the real paleo-geothermal gradient evolution path. Finally, we reconstructed the late Paleozoic-Cenozoic geothermal gradient history of the Ounan Sag, eastern Qaidam Basin (Fig. 9(b)).

#### 5. Results and interpretations

#### 5.1. Ro data

Fig. 4 presents 336  $R_0$  values and paleotemperatures obtained from wells/boreholes and outcrops in the Qaidam Basin. The figure shows that the  $R_0$  values of Carboniferous source rocks range from 0.86 % to 2.8 % and that those of Jurassic source rocks range from 0.3 % to 1.13 %. Notably, the average  $R_0$  value of the Carboniferous source rocks in a given area is higher than that of the Jurassic source rocks. Additionally, the maximum paleotemperatures of the Carboniferous source rocks range from 134.51 °C to 285.85 °C, while those of the Jurassic source rocks range from 51.47 °C to 169.52 °C. Specifically, the maximum paleotemperatures calculated from the Carboniferous source rocks in the eastern Qaidam Basin

are as follows:  $172.87 \,^{\circ}\text{C} - 218.05 \,^{\circ}\text{C}$  (well CY2),  $181.43 \,^{\circ}\text{C} - 240.12 \,^{\circ}\text{C}$  (section BSG), and  $210 \,^{\circ}\text{C} - 239 \,^{\circ}\text{C}$  (section GHNS).

Based on the two distinct ranges of maximum paleotemperatures, we propose that the heating processes of the Jurassic and Carboniferous source rocks can be categorized into two thermal systems. The Carboniferous source rocks attained their maximum paleotemperatures before the sedimentation of Jurassic rocks and did not undergo further increases thereafter. It is also inferred that a certain portion of the Carboniferous strata may have recorded at least one thermal event before the Jurassic.

# 5.2. Apatite (U-Th)/He data

For the eastern Ounan Sag, 20 single-grain AHe ages were obtained using samples from four outcrops (Table 2). The single-grain AHe ages range between 17.0  $\pm$  0.07 Ma and 76.5  $\pm$  0.32 Ma, which are considerably younger than their stratigraphic ages (350  $\pm$  5 Ma to 310  $\pm$  5 Ma).

The two factors that might be responsible for over-dispersion in AHe ages are (a) variations in crystal sizes that may have caused individual crystals to have different closure temperatures and yield different apparent ages; and (b) crystal-to-crystal variations in He diffusive behavior related to variations in radiation damage (Guenthner et al., 2013). For the sample GHNS, a considerably weak positive correlation is observed between AHe ages and eU, while no correlation exists with grain size (Fig. 6(a) and (b)). For the remaining samples, no correlation between the AHe ages and eU is observed (Fig. 6(a)), and there is also no correlation between age and grain size (Fig. 6(b)). These observations indicate that the samples have experienced a complex and protracted thermal history since the late Paleogene.

# 5.3. Zircon (U-Th)/He data

Among the grains collected from all four samples, 19 yield reproducible ZHe ages of  $289.3 \pm 1.29$  Ma  $\sim 200 \pm 0.85$  Ma (Table 3).

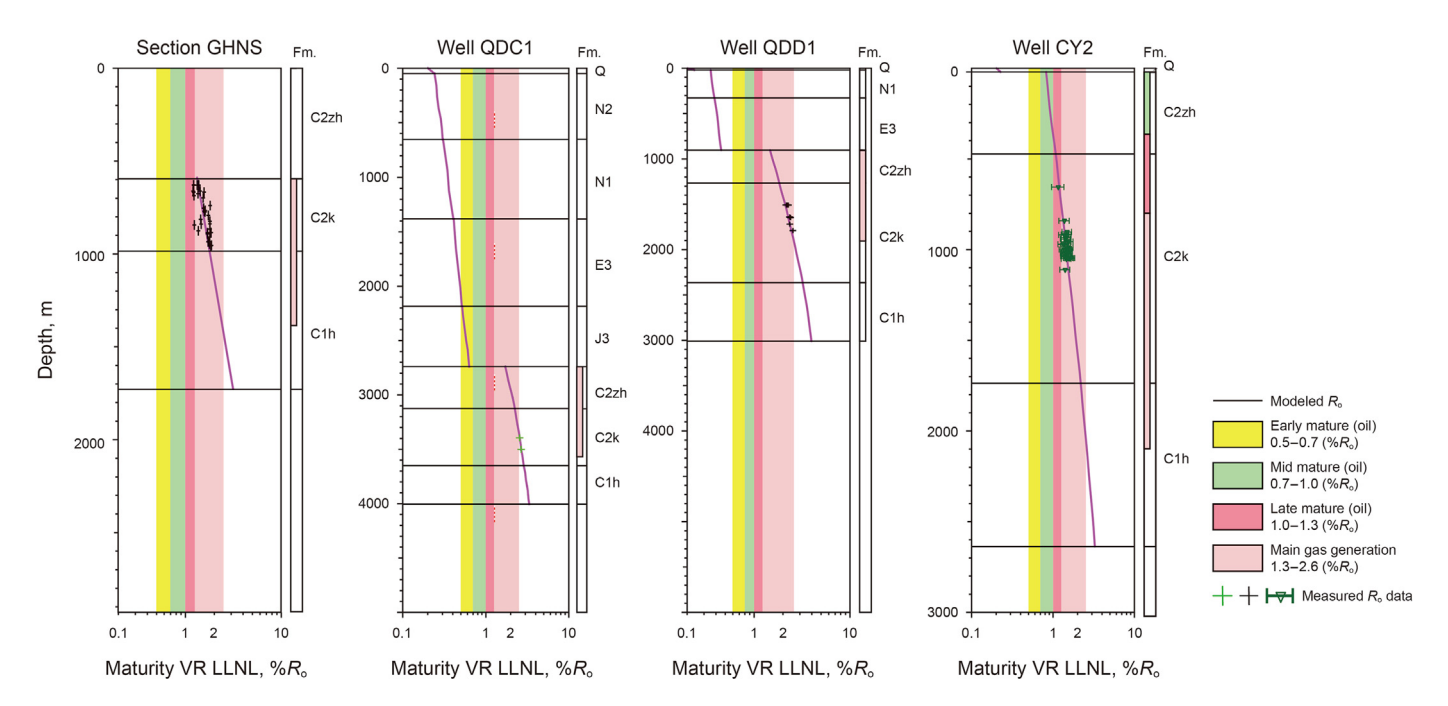


**Fig. 5.** Best-fit results of maturity value of simulation and measurement for the Carboniferous rocks of an outcrop section and three wells in the eastern Qaidam Basin. Here, the "Maturity VR LLNL" maturity conversion equation provided by the software was used for maturity ( $R_0$ ) calculation for the source rock interval. Maturity VR LLNL = maturity calculated by the Easy%  $R_0$  model, a simplified version of the VITRIMAT program of the Lawrence Livermore National Laboratory (LLNL).

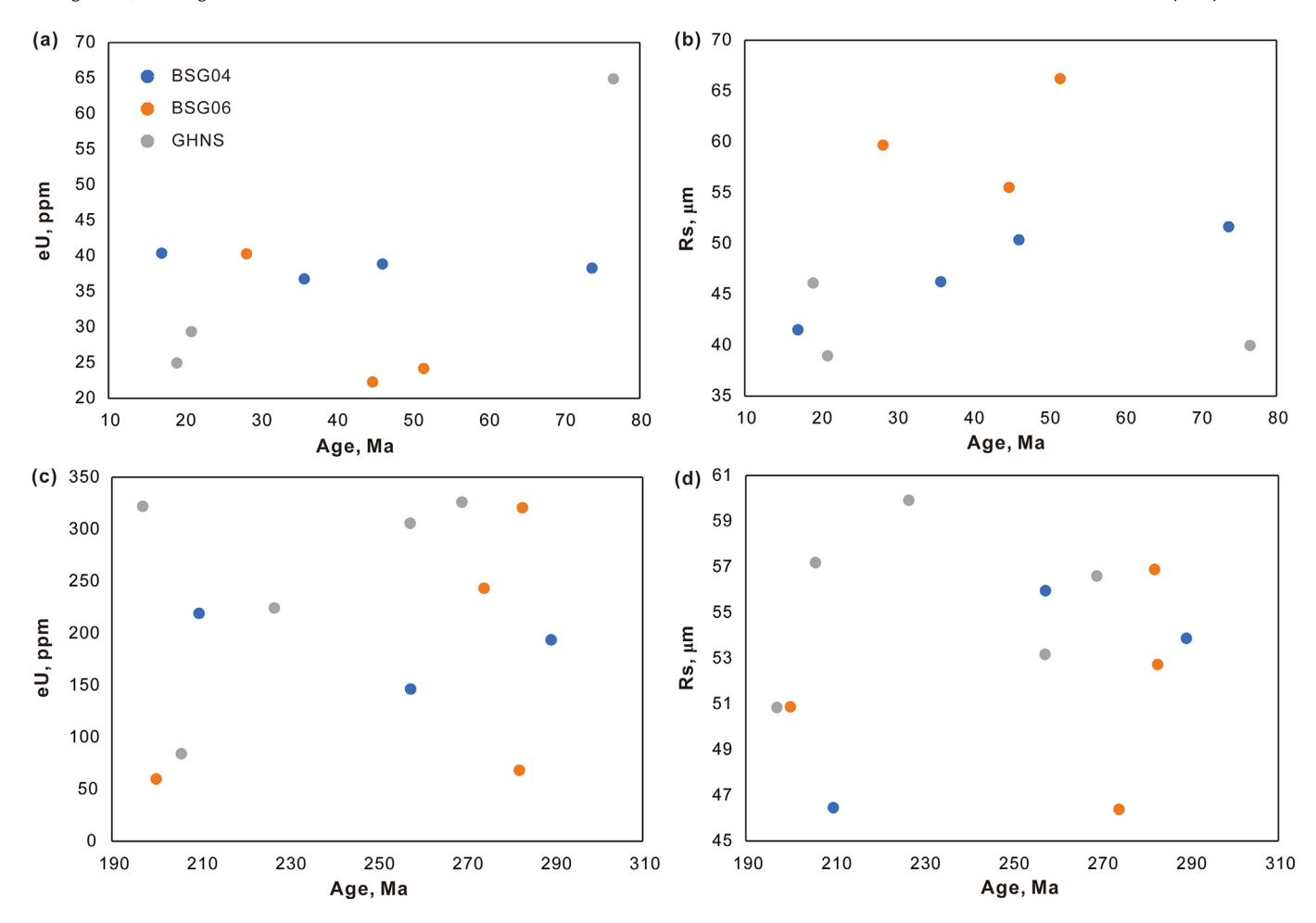


Fig. 6. Single AHe age versus eU content (a) and grain size (b); single ZHe age versus eU content (c) and grain size (d).

All the single-grain ZHe ages are younger than their stratigraphic ages, indicating heating to temperatures within the partial retention zone (130–210  $^{\circ}$ C).

The spherical radius of grains and radiation damage may primarily contribute to some age dispersion (Guenthner et al., 2017). On the one hand, after discarding the younger-age grain with a relatively high eU content, the sample GHNS exhibits a negative correlation with eU (Fig. 6(c)) and no correlation with the grain radius (Fig. 6(d)). On the other hand, no correlation between the ZHe ages and eU is observed in the remaining samples (Fig. 6(c)), and there is also no correlation between age and grain size (Fig. 6(d)). Negative age-eU correlations may indicate that some grains have experienced high damage amounts beyond the threshold, resulting in increased diffusivity (or decreasing closure temperatures) with increasing radiation damage (Guenthner et al., 2017). Overall, these results indicate that the ZHe samples in the eastern Qaidam Basin experienced a protracted thermal history from the late Paleozoic to the Mesozoic. In addition, all samples have experienced <sup>4</sup>He diffusion in the early Triassic, and the early thermal information has been reset.

# 5.4. Thermal history modeling

All thermal history modeling results produce goodness of fit (GOF) values > 0.9 (Fig. 7). The overall trend of the joint simulations (AHe and ZHe) from three samples obtained from the eastern Ounan Sag, eastern Qaidam Basin, is relatively similar. Three

models reveal a heating stage during the late Carboniferous to midlate Permian (~320–255 Ma), indicating these samples were continually deposited and heated above the temperature of ~200 °C (Fig. 7). Then, a significant cooling event began at ~252–245 Ma, with an initial temperature of ~190–150 °C, followed by cooling to ~80 °C at ~200 Ma with a cooling rate of ~2.5 °C/Ma (Fig. 9(a)). Three models also exhibited a reheating trend since the early Jurassic (~195 Ma) to the late Cretaceous (~80 Ma) reaching temperatures ranging from ~80 to 110 °C, within the temperature of AFT partial annealing zone (Gleadow et al., 2002). The BSG04, BSG06, and GHNS samples exhibited the onset time of the second cooling stage at ~93–80 Ma, followed by a further decrease to ~50 °C at ~55–38 Ma (Fig. 9(a)), maintaining a steady cooling status since then.

# 5.5. Basin modeling

As Fig. 8 shows, the reconstructed burial and thermal histories indicate that the Carboniferous strata in this study area underwent rapid burial and intense uplift from the late Paleozoic to Mesozoic. For the outcrop section model (GHNS), the burial and temperature trends show that the  $C_1h$  Formations have been heated to the maximum temperature of ~200 °C at the end of the Permian with a maximum burial depth of ~4000 m (Fig. 8(a)). For the three wells models, the value of maximum temperature and burial depth were moderately higher. From the early Carboniferous, the QDC1 model illustrates continuous subsidence, followed by reaching a

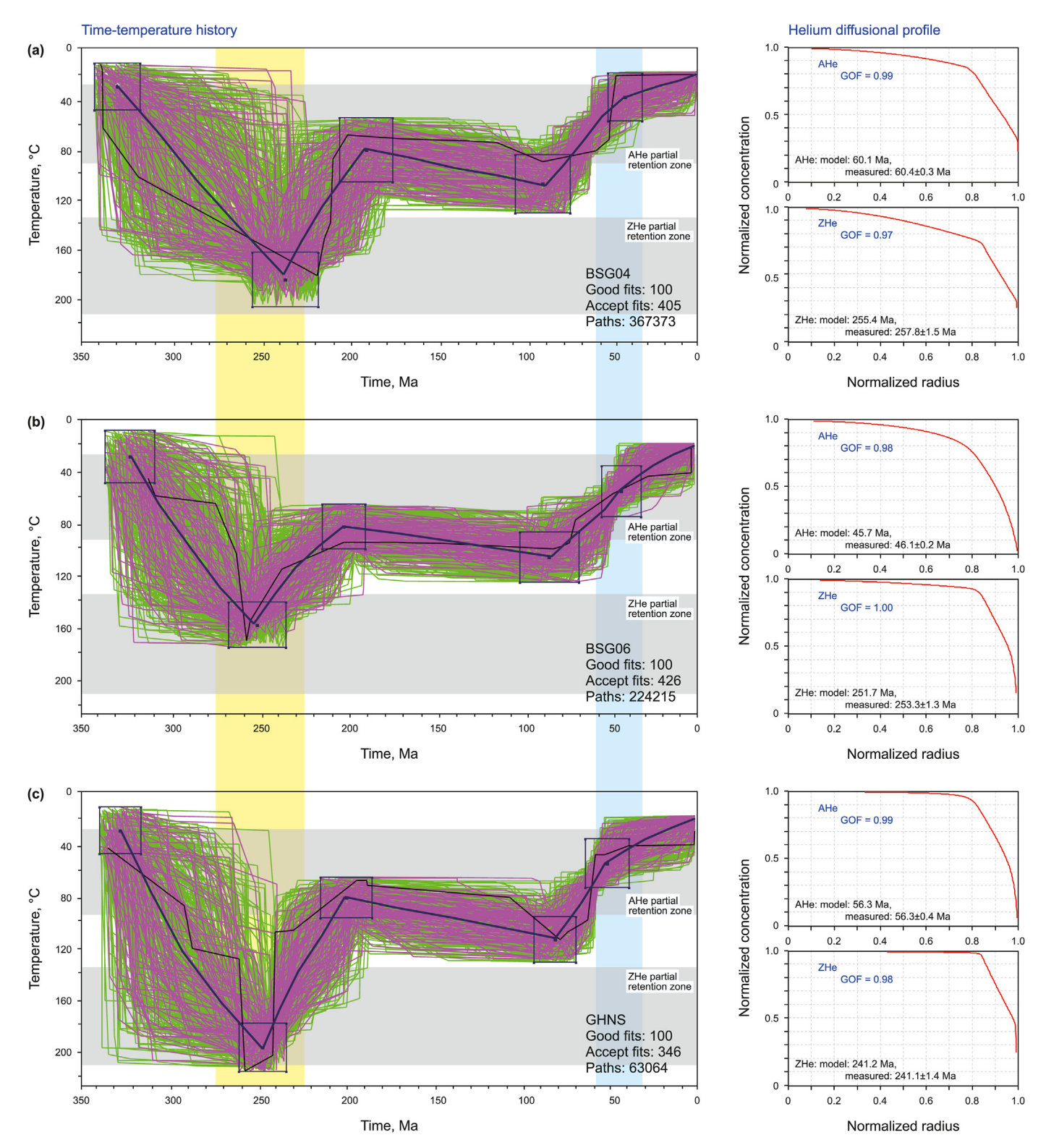


Fig. 7. Thermal history modeling of AHe and ZHe ages for the samples in the eastern Ounan Sag. These three models were originated from this study. The purple lines represent a good fit; the green lines represent an acceptable fit. The left figures show the attempted temperature paths. The thick blue line represents the weighted mean path and the thick black line represents the best fit. The right cure graph indicates a progression of the He concentrations from the core to the rim in a single grain (Ketcham, 2016). GOF represents the goodness of fit.

maximum burial depth in the middle Permian for the C1h Formations. Notably, the C1h Formations experienced a protracted heating episode, reaching a maximum temperature of 240  $\pm$  10  $^{\circ}C$  at

~260 Ma (Fig. 8(b)). The QDD1 model suggests a slower subsidence, with an increasing burial depth that led to a maximum temperature of ~245  $^{\circ}$ C at the end of the Permian (~250 Ma) for the C<sub>1</sub>h

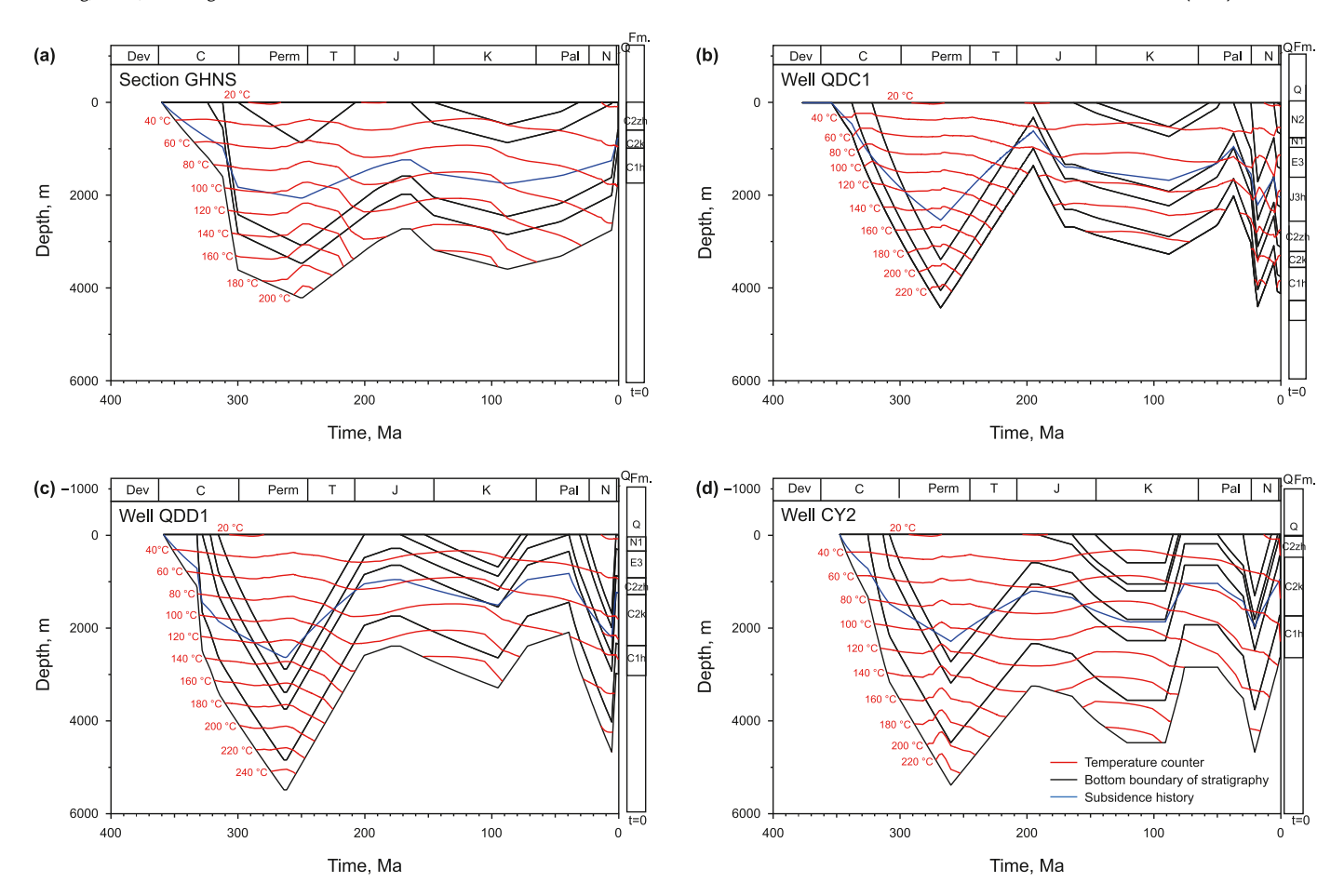


Fig. 8. Modeled burial history and corresponding thermal histories of the Carboniferous source rocks from an outcrop section and three different wells.

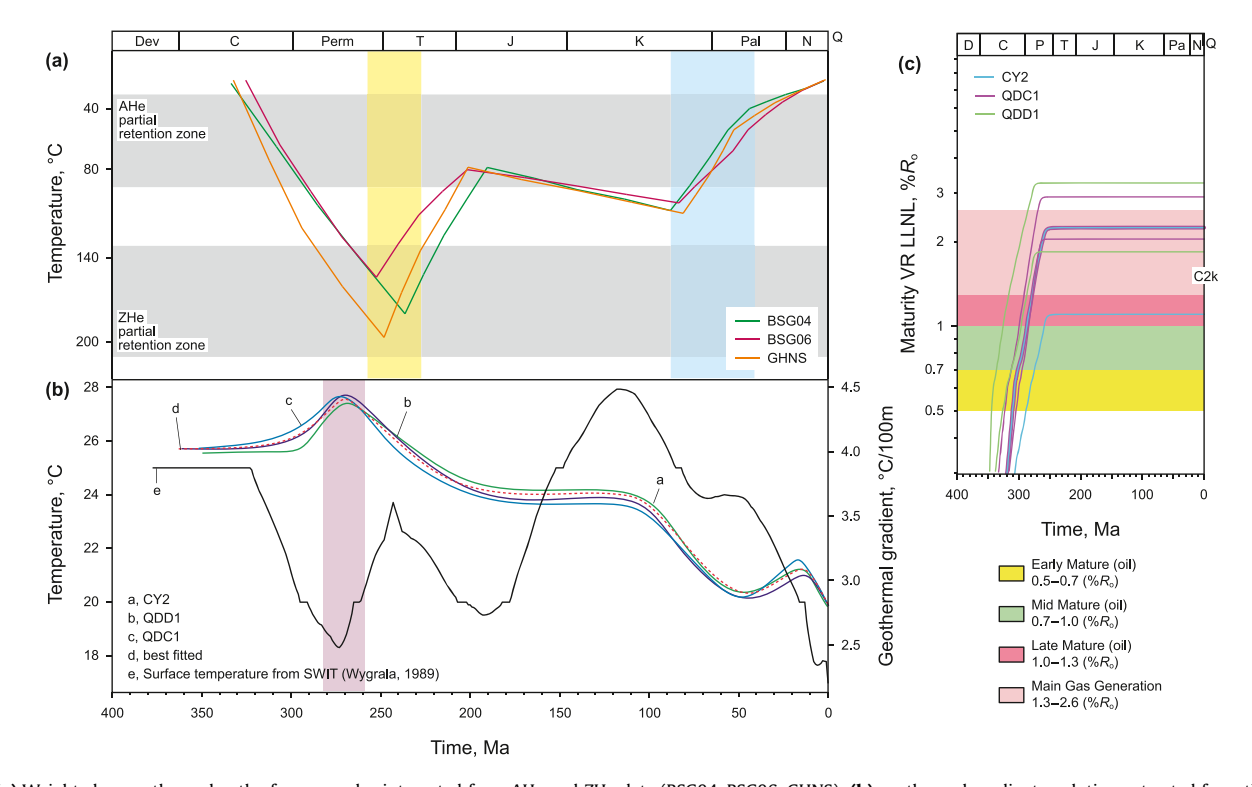


Fig. 9. (a) Weighted mean thermal path of our samples integrated from AHe and ZHe data (BSG04, BSG06, GHNS); (b) geothermal gradient evolution extracted from three-well modeling and the best fitting; (c) the source rock maturation histories of three wells.

Formations (Fig. 8(c)). Analysis of the burial—thermal model of the CY2 well indicates that the burial depth increased at a rate of 52 m/ Ma, with the increasing temperature at the bottom of the  $C_1h$  Formations at ~350–250 Ma (Fig. 8(d)). The maximum temperature was ~230 °C for the  $C_1h$  Formations, which is similar to those of the QDC1 and QDD1 models. All four models show that an exhumation/cooling event occurred from the end of the Paleozoic to Mesozoic time (Fig. 8(b), (c), and (d)).

The  $C_1h$  Formations cooled to  $130 \pm 10$  °C, and the burial depth decreased to ~3600 m at ~195 Ma, followed by a moderate reheating period below 180 °C from ~200 to 90 Ma. Notably, all three well models indicate that the Carboniferous strata experienced reburial events during the late Mesozoic to late Cenozoic. This resulted in at least two major reheating events concentrated since the early Jurassic (~198 Ma), with maximum burial depths of ~4800 m and maximum temperatures of ~140 °C. However, the outcrop section model has not recorded any reburial and/or reheating processes in the Cenozoic time. This model shows a similar trend to that of outcrop sample thermal modeling (Fig. 7), displaying continuous cooling since the late Cretaceous (~93 Ma).

The paleo-geothermal gradient increased from the early Carboniferous (~350 Ma) and reached a peak of ~43–44 °C/km in the late Permian in the Ounan Sag, eastern Qaidam Basin. The paleo-geothermal gradient began to decrease to ~36 °C/km at ~200 Ma. Then it gradually remained at ~35 °C/km until ~100–90 Ma. During the late Cretaceous to the late Paleocene, the paleo-geothermal gradient rapidly decreased and reached its minimum value of ~29.5 °C/km at ~50 Ma. During the Cenozoic era, the paleo-geothermal gradient gradually increased to ~31 °C/km at ~20–16 Ma. Then it decreased to its present-day value of ~28 °C/km (Li et al., 2017) (Fig. 9(b)).

# 6. Discussions

6.1. Exhumation/cooling events and their controlling factors in the eastern Qaidam Basin

# 6.1.1. Early Mesozoic (possibly end-Paleozoic to Mesozoic) time

Based on thermal history inversion results using AHe and ZHe data, we found evidence for an exhumation/cooling event in the Ounan Sag, eastern Qaidam Basin from the late Permian to the mid-Triassic (Fig. 9(a)). This cooling process was also recorded by the ZFT and ZHe ages in the SHG area (~275–254 Ma) (Li et al., 2015; Liu et al., 2020b). However, the results in the Ounan Sag differ from those in the Dulan area reported by Liu et al. (2020b) (~238 Ma). In the surrounding orogenic systems, the Triassic tectonic deformation event could be indicated by the sericite 40Ar/39Ar ages (~245–236 Ma) in the Zongwulong tectonic belt (Peng, 2015), and mica <sup>40</sup>Ar/<sup>39</sup>Ar ages of ~224–212 Ma in the East Kunlun Orogenic systems (Liu et al., 2005; Wang et al., 2016). This event could also be confirmed by the regional unconformities and the NNW-trending paleocurrents shown in the lower Triassic boulder beds (e.g., Liu et al., 2020b). We speculate that the main factor causing this event was the closure of the Paleo-Tethys Ocean and the resulting collision between the Kunlun-Qaidam arc and Bayanhar Terrane occurred in the Triassic (Zhao et al., 2018; Sun et al., 2022). In response to this collisional orogenesis, intense orogenic unroofing took place in the broad Kunlun-Qaidam arc (Dong et al., 2018; Li et al., 2022), where the lower crust thickened significantly (Xia et al., 2014) (Fig. 10(a)). Therefore, the Dulan area recorded the exhumation/cooling event at the time when the magmatic flare-up took place in the surrounding orogenic systems contemporaneously. For the exhumation/cooling in the Ounan Sag, we proposed an intense forebulge flexural elevation that took place earlier than the unroofing events in the orogenic systems. This could also be

proved by the thick erosion of the Permian strata in the eastern Qaidam Basin and the gradual expansion of the Zongwulong continental rift (Sun et al., 2022; Zhong et al., 2024a). During the Permian, the Carboniferous strata in the Ounan Sag were continuously buried in the greater Qaidam epicontinental sea (Sun et al., 2022) (Fig. 10(a)).

#### 6.1.2. Late Mesozoic to Cenozoic time

Our new AHe ages and joint thermal inversion models present the main exhumation/cooling stage during the late Cretaceous to Eocene (~85-35Ma) (Fig. 9(a)). This finding is consistent with the previous AFT thermal modeling (Wang et al., 2022). This exhumation/cooling event may be related to the collision of the Gangdise-Nyaingentanglha Terrane and the Eurasian Plate (Pan et al., 2012; Wang et al., 2022). We speculate that this tectonic process formed the prototype of the present-day Olongbuluke uplift. Given that the study area is confined by the Cenozoic reactivated reverse faults (i.e., Ounan Fault, Liu et al., 2020b), these models may also align with the initial rapid cooling events from the apatite helium age/ depth transects in the hanging wall of the West Qinling thrust (~45-50 Ma) and the North Qaidam thrust (~35 Ma) (Clark et al., 2010). This accelerated exhumation likely signalled the first major thrust activity in northeastern Tibet following the India-Eurasia collision, which has been described by considering the role of strength heterogeneities in the continental lithosphere or basal tractions induced by mantle flow (Meng and Fang, 2008; Clark et al., 2010) (Fig. 10(b)). We speculate that this also could be the primary factor contributing to the differential thermal evolution in the eastern area of eastern Oaidam Basin. As the Ounan thrust fault became active from the end of Cretaceous to the Paleogene, the studied area experienced a cooling process in response to this. The paleo-topography of GHNS area may be relatively high after this exhumation, and thereby samples located at the hanging wall have not been reburied in later stages. In contrast to the residual thickness of the Carboniferous strata, we found that the residue in the outcrop is relatively thinner than those in the adjacent wells, i.e., C1h Formations of 744.9 m and C2k Formations of 389.9 m for the GHNS section (QBGMR, 1978); C2k Formations of 682m for the QDC1 well. Combined with the modeling results, these indicate that the GHNS area experienced a weak amplitude of denudation since the early Miocene, as also featured by the AFT thermal models from Li et al. (2015, 2017). In addition, this cooling process was also supported by the field deformation and seismic reflection data: the northern Qaidam thrust belts mainly reactivated at ca. 16 Ma, forming the Oulongbuluke and Aimunike uplifts and that this thrust belt development lasted until the late Quaternary (e.g., Bush et al., 2016; Mao et al., 2020; Wang et al., 2024). In contrast, as QDC1 and QDD1 wells located at the footwall of the thrust fault systems, the thermal modeling results exhibited reburial processes since the Eocene (sec tion 5.2.2).

6.2. Heating process and its potential genesis in the eastern Qaidam Basin

# 6.2.1. Late Paleozoic time

Based on the initial temperature model derived from vitrinite reflectance data, we conducted joint inversions of the AHe and ZHe ages and obtained the thermal history of the eastern Ounan Sag of the eastern Qaidam Basin. Notably, the time-temperature variations in the heating process of the Carboniferous strata are roughly the same for individual samples. Our modeling results show that since the early Carboniferous (~350 Ma), almost all thermal inversion models record a basin-wide heating event, which lasted from the Carboniferous (~350 Ma) to the late Permian (~252–245 Ma) and reached a maximum temperature of ~180  $\pm$  20 °C. Notably, the

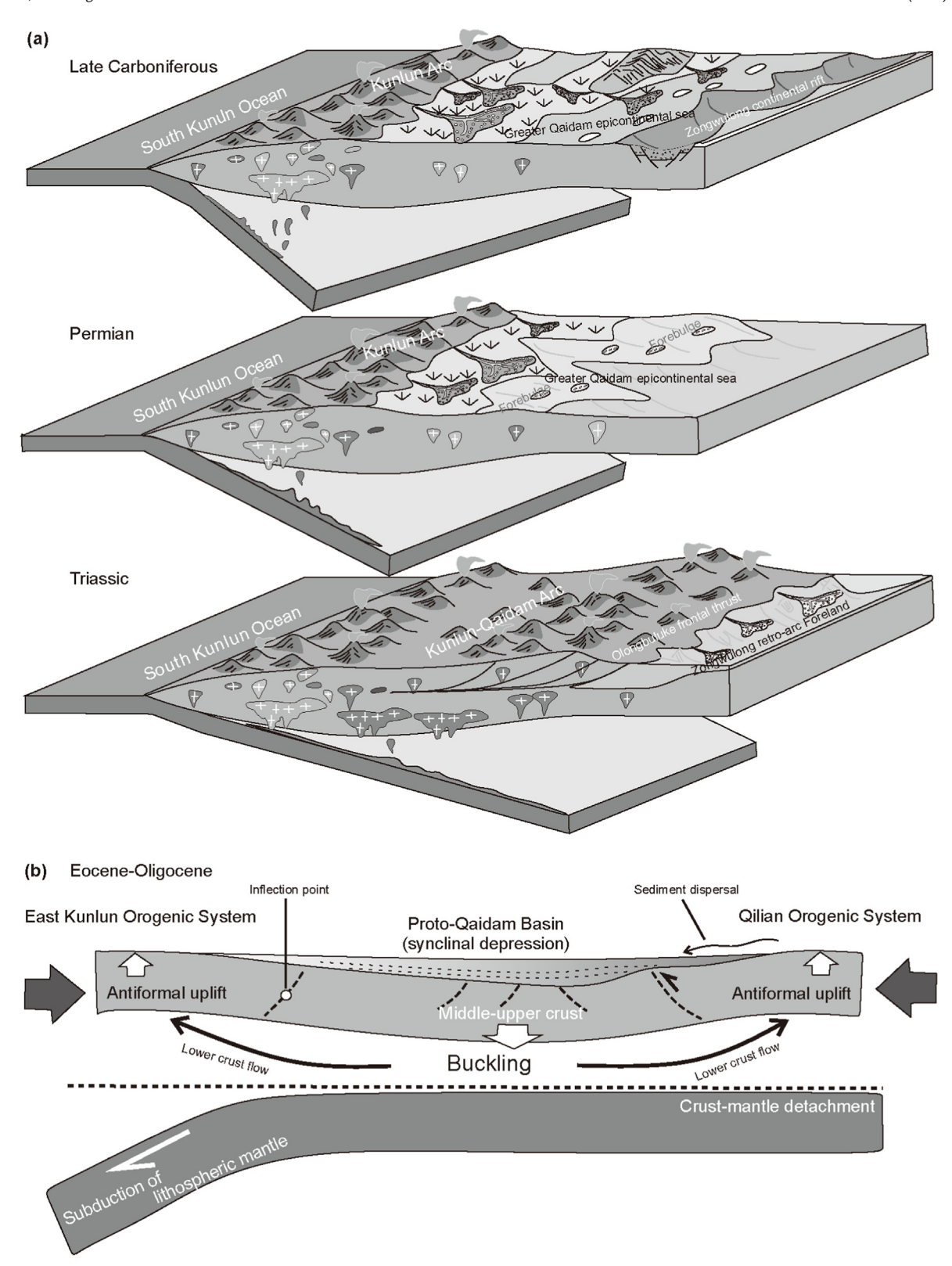


**Fig. 10.** (a) Theoretical block models show the tectono-thermal evolution of the eastern Qaidam basin and its surrounding orogenic systems, and indicate multiple stages of evolution in paleogeography from the Carboniferous to the Triassic (modified from Sun et al., 2022); (b) two-dimensional model depicts the formation of the eastern Qaidam Basin during the Eocene to the late Oligocene (modified from Meng et al., 2008). See the main text for details.

individual thermal model reaching its maximum temperature was later than the Carboniferous strata reaching their peak paleogeothermal gradient: the maximum paleogeothermal gradient fitted by forward modeling reached  $\sim$ 43–44 °C/km at  $\sim$ 265  $\pm$  10 Ma.

As shown in the basin modeling results (Fig. 8), the heating process during this period can be explained by the continuously increasing burial depth of the Carboniferous strata (Zhong et al., 2024a). However, we can now propose another genesis. It is widely acknowledged that the thermal signatures in the eastern Qaidam Basin are mainly controlled by the amalgamation of three microblocks and a magmatic flare-up (Li et al., 2017; Sun et al., 2022). The arc magmatism in the Kunlun-Qaidam arc terrane since the early Carboniferous (~350 Ma) has been attributed to the continuous northward subduction of the South Kunlun Ocean (Pan et al., 2012; Yan et al., 2014; Jiao et al., 2020). At this time, the Zongwulong Rift formed within the retroarc zone (Chen et al., 2016). The latest detrital zircon spectrum age of ~330 Ma indicates that the Carboniferous subsidence was affected by near-arc magmatic activity in the eastern Qaidam Basin, but there was probably weak intrusion of magmatic rocks in the arc-shaped terrane due to continuous subduction (Sun et al., 2022). Additionally, considering the previous low-frequency occurrence of magmatic records during ~360-300 Ma and that volcanic eruptions were distributed sporadically across the northern basin (Zhong et al., 2024b), thermal events during the Carboniferous were relatively infrequent. In this case, we speculate that the Carboniferous strata did not reach their maximum paleotemperature at this time due to the paucity of magmatism. Subsequently, in the mid-late Permian, igneous rocks, especially granitic intrusive rocks, formed abundantly in the peripheral orogenic systems. The ~270–260 Ma feldspar granites in the Wulan area (QBGMR, 1991; Guo et al., 2009; Chen et al., 2015; Wu et al., 2016) may be related to the occurrence of thermal events in the eastern Ounan Sag and directly resulted in a heating event in the Carboniferous strata. The ~290-270 Ma granodiorites revealed by deep drilling in Luliangshan and other surrounding orogenic systems (Menold, 2006; Cheng et al., 2017) suggest that thermal events also occurred in the early to middle Permian in the western Ounan Sag. For the southern margin of the basin, the duration of the intrusion of igneous rocks lasted much longer (~269-240 Ma) (QBGMR, 1991; Gehrels et al., 2003; Chen et al., 2015); coincidently, this can also explain the longer heating time of the Carboniferous strata in the Dulan area. Sun et al. (2022) concluded that the large-scale intrusion of Permian magmas was related to slab breakoff, tearing or rollback of the Southern Kunlun oceanic lithosphere, which would have led to the upwelling of the asthenosphere below the Qaidam Terrane (Fig. 10(a)). Therefore, it is possible that the highest geothermal gradient reflected in the basin was related to the contemporaneous intrusion of plutons below or within the crust. Collectively, the mid-late Permian thermal event in the eastern Qaidam Basin could be attributed to plate dynamics, asthenospheric upwelling, and widespread intrusion of magmatic rocks or plutons (Fig. 10(a)).

# 6.2.2. Mesozoic-Cenozoic time

All inversion models in this study depict a main reheating trend during the Mesozoic (~190—90 Ma). These models depict a stage of quasi-isothermal quiescence during this period, characterized by a decreasing paleo-geothermal gradient evolution (Fig. 9). This may be related to the tectonic quiescence during this period instead of intense orogenesis or plate subduction (Cheng et al., 2019; Hu et al., 2020a). We speculate that the moderate reheating process could be attributed to the intermountain and shallow lake sedimentation, and the Carboniferous strata reburied to ~3000m above ~140 °C (Fig. 8(a)). The well models show that there was a period of reburial and reheating processes for the Carboniferous strata during the

middle and late Cenozoic (Fig. 9). This result can be attributed to the extensive sedimentation (>1.5 km) of the Shangganchaigou Formations and the relatively slower tectonic uplift in the eastern Qaidam Basin, as evidenced by growth strata and seismic data (Yin et al., 2008; Yu et al., 2017). This may have been influenced by the southward shift of the sedimentary center in the eastern Qaidam Basin before the deposition of the Shangyoushashan Formation, resulting in the accelerated reburial of Paleozoic strata in the Huobuxun Sag (~1.2 km) (Fang et al., 2007; Meng and Fang, 2008; Du et al., 2016; Cheng et al., 2021). In addition, some researchers believe that the growth of the Qaidam Basin may be explained by a foreland basin evolution model: either extension along the Ela Shan Fault shear zone or the exhumation of the Zongwulong Range, which formed a topographic load and caused local flexural subsidence (Wang et al., 2021, 2024). Therefore, the slight increase in the paleogeothermal gradient to ~32 °C/km from the Eocene to the end of the Oligocene (Fig. 9(b)) may be attributed to the extensive sedimentary load during this period (Fig. 10(b)).

### 6.3. Implication for the hydrocarbon generation

Hydrocarbon generation and expulsion from source rocks are integral components of the hydrocarbon accumulation process, and tectono-thermal evolution plays a critical role in these processes (e.g., Zheng et al., 2019; Hu et al., 2020b; Xu et al., 2021; Gao et al., 2022; Zhou et al., 2023). The study of the maturation evolution of source rocks is the basis for evaluating hydrocarbon generation and accumulation (Chang et al., 2018; Wang and Guo, 2021; Pang et al., 2024). Based on the new paleo-geothermal gradient history and uplift stages and amplitudes, we modeled the maturation evolution histories of the Carboniferous (Keluke Formations) source rocks, which are mainly distributed in the study area (Shi et al., 2022, 2023a, 2023b). The maturation modeling results from the well CY2 indicated that the maturation of the C2k Formation source rock in the western Ounan Sag increased quickly from the Carboniferous to late Permian and reached a maximum of 1.08-2.27 % at the end of Permian (~252 Ma) (Fig. 9(c)). The most C2k Formations in this area has been reached the gas generation stage during this period, while the upper part of C2k Formation remained in the late mature stage. For the eastern Ounan Sag, the wells QDC1 and QDD1 indicate that the upper member of C2k Formations reached the main gas generation stage earlier than that of the well CY2 in the late Permian, revealed by the 1.77–3.18 % of  $R_0$ .

There are many structural evolution models indicating that during the Cenozoic time, multi-stage tectonism occurred in the studied area, and the fault activity was obviously enhanced (e.g., Li et al., 2015; Cheng et al., 2016). However, they have a rather limited impact on the Carboniferous residue (Cheng et al., 2016; Guo et al., 2022; Zhong et al., 2024a). Moreover, basin modeling results indicate that the late burial depth did not exceed the early episode that terminated the hydrocarbon generation. Thereby, secondary hydrocarbon generation did not occur. It is noteworthy that the primary hydrocarbon reservoirs in the early stage may have been adjusted and reconstructed by the later tectonism. However, the residual primary reservoirs, traps developed at the later stage, may accumulate the redistributed oil and gas (Guo et al., 2022). The widely distributed Carboniferous source rocks, especially the upper members of C2k Formations, maintain significant residual thickness in the Ounan (Delingha) Sag (Cheng et al., 2016; Liu et al., 2012, 2020a), where tectonic activities were weak at the later stages, which may have good resources potential in the deep. Therefore, there is good potential for further petroleum exploration of the upper members of C<sub>2</sub>k Formations in the eastern Qaidam Basin.

#### 7. Conclusions

In this study, we present new AHe and ZHe thermochronological data for the Ounan Sag, eastern Qaidam Basin. Based on the  $R_0$  initial thermal model and thermochronological ages, we employ thermal inversion and basin modeling of the study area to provide a detailed understanding of the thermal evolution that has occurred since the late Paleozoic. Here are the main conclusions.

- (1) The AHe data from three outcrop samples range from 17 Ma to 76.5 Ma, and the ZHe data range from 200 Ma to 289.3 Ma. The thermal modeling results revealed two main cooling events that occurred from the end of Permian to Triassic, and the late Cretaceous to Eocene. The first cooling event might be resulted from intense forebulge flexural elevation and orogen unroofing, which was likely related to the collision and orogenesis that occurred between the Kunlun-Qaidam arc and Bayanhar Terrane. The second stage was caused by the thrust fault activity, which may be related to the continental lithosphere or basal tractions induced by mantle flow, following the India—Eurasia collision.
- (2) We identified consistent heating during the late Paleozoic, reaching the maximum paleotemperature (~230 °C) and geothermal gradient peak (~43–44 °C/km) in the late Permian, which may be attributed to the rapid subsidence of the overlying strata, and the widespread intrusion of plutons caused by asthenosphere upwelling below the Qaidam Terrane. We also observed a reheating event in the Eocene with paleotemperatures less than 180 °C and paleogeothermal gradient of ~31 °C/km, which were probably related to local flexural subsidence. Our observations suggest that the source rocks in the most upper member of C<sub>2</sub>k Formations in the Ounan Sag reached the gas generation stage peak maturation stage during the late Permian.

# Data availability

Data will be made available on request.

# **CRediT authorship contribution statement**

Chang Zhong: Writing — original draft, Visualization, Software, Methodology, Investigation. Hui Shi: Writing — review & editing, Software, Methodology, Investigation, Formal analysis, Data curation. Xiao-Yin Tang: Funding acquisition, Resources, Supervision, Writing — review & editing. Hao Zhang: Writing — review & editing, Visualization, Validation, Supervision, Funding acquisition. Yuan-Yuan Yang: Resources, Methodology, Investigation. Jun-Jie Hu: Methodology, Investigation, Conceptualization. Xiao-Jie Wei: Visualization, Conceptualization, Jia-Qi Wang: Visualization, Software.

# **Declaration of competing interest**

The authors declare that they have no known competing financial interests or personal relationships that could have appeared to influence the work reported in this paper.

# Acknowledgments

This research was financially supported by grants from the Geological Survey Projects of China Geological Survey (grant nos. 20242065, 20230260), the Fundamental Research Fund of Chinese Academy of Geological Sciences (grant no. JKYQN202342) and the

National Natural Science Foundation of China (grant no. 41772272).

We would like to thank Roman Kislitsyn for his technical assistance with the apatite and zircon (U—Th)/He analyses. We also thank Li-Cheng Ma and Paul R. Eizenhöfer for their insightful discussions and comments. Our heartfelt gratitude is given to the editors and the reviewers for their scientific and linguistic revisions of the manuscript.

# Appendix A. Supplementary data

Supplementary data to this article can be found online at https://doi.org/10.1016/j.petsci.2024.05.011.

### References

- Ashrafi, T., Saberi, M.H., ZareNezhad, B., 2020. 1D and 2D basin modeling, in evaluating the hydrocarbon generation-migration-accumulation potential, at coastal Fars Area, Southern Iran. J. Petrol. Sci. Eng. 195, 107594. https://doi.org/10.1016/j.petrol.2020.107594.
- Barker, ChE., Pawlewicz, M.J., 1986. The correlation of vitrinite reflectance with maximum temperature in humic organic matter. In: Buntebarth, G., Stegena, L. (Eds.), Paleogeothermics: Evaluation of Geothermal Conditions in the Geological Past, Lecture Notes in Earth Sciences. Springer, Berlin, Heidelberg, pp. 79–93. https://doi.org/10.1007/BFb0012103.
- Barker, C.E., Goldstein, R.H., 1990. Fluid-inclusion technique for determining maximum temperature in calcite and its comparison to the vitrinite reflectance geothermometer. Geology 18 (10), 1003–1006. https://doi.org/10.1130/0091-7613(1990)018<1003:FITFDM>2.3.CO;2.
- Bush, M.A., Saylor, J.E., Horton, B.K., Nie, J., 2016. Growth of the Qaidam Basin during Cenozoic exhumation in the northern Tibetan Plateau: inferences from depositional patterns and multiproxy detrital provenance signatures. Lithosphere 8 (1), 58–82. https://doi.org/10.1130/L449.1.
- Cao, J., Bian, L., Liu, Y., Hu, K., Yang, S., Wang, L., Chen, Y., Sun, P., 2009. Hydrocarbon generation potential of middle and lower Jurassic source rocks in the northern margin of Qaidam Basin. Xinjing Pet. Geol. 30, 22–24, 1001-3873-(2009)01-0021-04 (in Chinese).
- Chang, J., Glorie, S., Qiu, N., Min, K., Xiao, Y., Xu, W., 2021. Late Miocene (10.0~6.0 Ma) rapid exhumation of the Chinese south tianshan: implications for the timing of aridification in the Tarim basin. Geophys. Res. Lett. 48 (3), e2020GL090623. https://doi.org/10.1029/2020GL090623.
- Chang, J., Qiu, N., Liu, S., Cai, C., Xu, Q., Liu, N., 2019. Post-Triassic multiple exhumation of the Taihang Mountains revealed via low-T thermochronology: implications for the paleo-geomorphologic reconstruction of the North China Craton. Gondwana Res. 68, 34–49. https://doi.org/10.1016/j.gr.2018.11.007.
- Chang, J., Qiu, N., Xu, W., 2017. Thermal regime of the Tarim basin, northwest China: a review. Int. Geol. Rev. 59 (1), 45–61. https://doi.org/10.1080/00206814.2016.1210546.
- Chang, J., Qiu, N., Zhao, X., Shen, F., Liu, N., Xu, W., 2018. Mesozoic and Cenozoic tectono-thermal reconstruction of the western Bohai Bay Basin (East China) with implications for hydrocarbon generation and migration. J. Asian Earth Sci. 160, 380–395. https://doi.org/10.1016/j.jseaes.2017.09.008.
- 160, 380—395. https://doi.org/10.1016/j.jseaes.2017.09.008.

  Chang, J., Yang, X., Qiu, N., Min, K., Li, C., Li, H., Li, D., 2022. Zircon (U-Th)/He thermochronology and thermal evolution of the Tarim basin, western China. J. Asian Earth Sci. 230, 105—210. https://doi.org/10.1016/j.jseaes.2022.105210.
- Cheng, F., Jolivet, M., Guo, Z., Lu, H., Zhang, B., Li, X., Zhang, D., Zhang, C., Zhang, H., Wang, L., Wang, Z., Zhang, Q., 2019. Jurassic—Early Cenozoic tectonic inversion in the Qilian Shan and Qaidam Basin, North Tibet: new insight from seismic reflection, isopach mapping, and drill core data. J. Geophys. Res. Solid Earth 124, 12077—12098. https://doi.org/10.1029/2019JB018086
- 12077—12098. https://doi.org/10.1029/2019JB018086.
  Cheng, F., Jolivet, M., Guo, Z., Wang, L., Zhang, C., Li, X., 2021. Cenozoic evolution of the Qaidam basin and implications for the growth of the northern Tibetan plateau: a review. Earth Sci. Rev. 220, 103730. https://doi.org/10.1016/j.earscirev.2021.103730.
- Cheng, F., Jolivet, M., Hallot, E., Zhang, D., Zhang, C., Guo, Z., 2017. Tectono-magmatic rejuvenation of the Qaidam craton, northern Tibet. Gondwana Res. 49, 248–263. https://doi.org/10.1016/j.gr.2017.06.004.
- Cheng, R., Xiao, Y., Lin, H., Liu, Z., Wang, D., Li, J., Chai, X., Ding, L., 2016. A study of Carboniferous stratigraphic distribution and controlling factors in the eastern section of North Qaidam. Earth Sci. Front. 23, 75–85 (in Chinese).
- Chen, S., Bi, M., Sun, J., Zhang, Y., Zhuang, Y., Liu, J., Wang, F., Ma, S., 2016. Mixed sedimentary characteristics and controlling factors of upper paleozoic Group in northern Qaidam Basin. Geol. Bull. China 35 (2–3), 282–292 (in Chinese).
- Chen, X., Gehrels, G., Yin, A., Zhou, Q., Huang, P., 2015. Geochemical and Nd—Sr—Pb—O isotopic constrains on Permo—Triassic magmatism in eastern Qaidam Basin, northern Qinghai-Tibetan plateau: implications for the evolution of the Paleo-Tethys. J. Asian Earth Sci. 114, 674—692. https://doi.org/10.1016/j.jseaes.2014.11.013.
- Chen, Y., Zhang, S., 2011. Organic Geochemical Characteristics of Middle Jurassic Source Rocks in Delingha Depression, Qaidam Basin, vol. 38. Journal of Chengdu University of Technology (Natural Science Edition), pp. 191–198 (in Chinese).

Clark, M.K., Farley, K.A., Zheng, D., Wang, Z., Duvall, A.R., 2010. Early Cenozoic faulting of the northern Tibetan Plateau margin from apatite (U—Th)/He ages. Earth Planet Sci. Lett. 296, 78—88. https://doi.org/10.1016/j.epsl.2010.04.051.

- Dang, H., 2019. Characteristics and Occurrence Rules of Oil Shale in the Second Member of the Middle Jurassic Shimengou Formation in the Northern Margin of Qaidam Basin. Master's dissertation. Jilin University (in Chinese).
- Darby, B.J., Ritts, B.D., Yue, Y., Meng, Q., 2005. Did the Altyn Tagh Fault extend beyond the Tibetan plateau? Earth Planet Sci. Lett. 240 (2), 425–435. https://doi.org/10.1016/j.epsl.2005.09.011.
- Dong, Y., He, D., Sun, S., Liu, X., Zhou, X., Zhang, F., Yang, Z., Cheng, B., Zhao, G., Li, J., 2018. Subduction and accretionary tectonics of the East Kunlun orogen, western segment of the Central China Orogenic System. Earth Sci. Rev. 186, 231–261. https://doi.org/10.1016/j.earscirev.2017.12.006.
- Dong, Y., Sun, S., Santosh, M., Zhao, J., Sun, J., He, D., Shi, X., Hui, B., Cheng, C., Zhang, G., 2021. Central China orogenic belt and amalgamation of East asian continents. Gondwana Res. 100, 131–194. https://doi.org/10.1016/i.gr.2021.03.006.
- Duan, H., Zhong, J., Wang, Z., Ma, F., Yin, C., Wen, Z., 2006. Evaluation of carboniferous source rocks in eastern Qaidam Basin. Geol. Bull. China 25 (9–10), 1135–1142 (in Chinese).
- Du, Z., Fan, L., Wu, G., Wei, H., Meng, Q., 2016. Cenozoic architecture and structural development of the eastern Qaidam basin. Chin. J. Geophys. 59 (12), 4560–4569. https://doi.org/10.6038/cjg20161218 (in Chinese).
- Eizenhöfer, P.R., Glotzbach, C., Büttner, L., Kley, J., Ehlers, T.A., 2021. Turning the orogenic switch: slab-reversal in the eastern Alps recorded by low-temperature thermochronology. Geophys. Res. Lett. 48 (6), e2020GL092121. https://doi.org/ 10.1029/2020GL092121.
- Eizenhöfer, P.R., Glotzbach, C., Kley, J., Ehlers, T.A., 2023. Thermo-kinematic evolution of the eastern European Alps along the TRANSALP transect. Tectonics 42 (4), e2022TC007380. https://doi.org/10.1029/2022TC007380.
- Fang, C., Li, F., Meng, L., Li, L., Lin, H., Yang, Y., 2012. Evaluation of Middle Jurassic source rocks in Hongshan fault depression, northern margin of Qaidam Basin. Nat. Gas Geosci. 23 (5), 856–861, 1672-1926(2012)05-0856-06 (in Chinese).
- Fang, X., Zhang, W., Meng, Q., Gao, J., Wang, X., King, J., Song, C., Dai, S., Miao, Y., 2007. High-resolution magnetostratigraphy of the neogene Huaitoutala section in the eastern Qaidam Basin on the NE Tibetan plateau, Qinghai province, China and its implication on tectonic uplift of the NE Tibetan plateau. Earth Planet Sci. Lett. 258 (1), 293–306. https://doi.org/10.1016/j.epsl.2007.03.042.
- Farly, A., 2002. (U-Th)/He dating, techniques, calibrations, and applications. Rev. Mineral. Geochem. 47 (1): 819—844. doi: https://doi.org/10.2138/rmg.2002.47.
- Flowers, R.M., Ketcham, R.A., Shuster, D.L., Farley, K.A., 2009. Apatite (U—Th)/He thermochronometry using a radiation damage accumulation and annealing model. Geochem. Cosmochim. Acta 73 (8), 2347–2365. https://doi.org/10.1016/j.gca.2009.01.015.
- Fu, X., Rao, D., Qin, J., Shen, B., Xu, J., Yang, Z., 2014. Geological conditions of shale oil formation in dameigou formation of middle jurassic in the northern margin of Qaidam Basin. Lithol. Reservoirs 26 (6), 20–33, 1673-8926(2014)06-0020-08 (in Chinese).
- Gao, P., Li, Z., Miao, M., Li, S., Zhang, H., 2022. Tectono-thermal evolution and its significance of hydrocarbon exploration in the Fuyang Sag, Southern North China Basin: a case study of well WFD-1. Front. Earth Sci. 9, 786849. https:// doi.org/10.3389/feart.2021.786849.
- Gehrels, G.E., Yin, A., Wang, X., 2003. Magmatic history of the northeastern Tibetan Plateau. J. Geophys. Res. Solid Earth 108 (B9), 2423. https://doi.org/10.1029/2002/B001876.
- Gleadow, A.J.W., Belton, D.X., Kohn, B.P., Brown, R.W., 2002. Fission track dating of phosphate minerals and the thermochronology of apatite. Rev. Mineral. Geochem. 48 (1), 579–630. https://doi.org/10.2138/rmg.2002.48.16.
- Gong, H., Chen, Z., Hu, Y., Li, L., Li, S., Zheng, E., Han, X., 2007. Meso-Neoproterozoic tectono-thermal evolution in the northern margin of North China Craton: constraints from zircon (U-Th)/He ages. J. Geomechanics 28 (1), 113–125. https://doi.org/10.12090/j.issn.1006-6616.2021042 (in Chinese).
- Guenthner, W.R., Reiners, P.W., Drake, H., Tillberg, M., 2017. Zircon, titanite, and apatite (U-Th)/He ages and age-eU correlations from the Fennoscandian Shield, southern Sweden. Tectonics 36 (7), 1254–1274. https://doi.org/10.1002/2017TC004525.
- Guenthner, W.R., Reiners, P.W., Ketcham, R.A., Nasdala, L., Giester, G., 2013. Helium diffusion in natural zircon: radiation damage, anisotropy, and the interpretation of zircon (U-Th)/He thermochronology. Am. J. Sci. 313 (3), 145–198. https://doi.org/10.2475/03.2013.01.
- Guo, A., Zhang, G., Qiang, J., Sun, Y., Li, G., Yao, A., 2009. The Indosinian Zongwulong orogenic belt in the northeast margin of the Tibetan Plateau. J. Petrol. 25 (1), 1–12, 1000-0569/2009/025(01)-0001-12 (in Chinese).
- Guo, Y., Cao, J., Liu, R., Wang, H., Zhang, H., 2022. Hydrocarbon accumulation and alteration of the Upper Carboniferous Keluke Formation in the eastern Qaidam Basin: insights from fluid inclusion and basin modeling. J. Petrol. Sci. Eng. 211, 110–116. https://doi.org/10.1016/j.petrol.2022.110116.
- Gusmeo, T., Schito, A., Corrado, S., Alania, V., Enukidze, O., Zattin, M., Pace, P., Cavazza, W., 2022. Tectono-thermal evolution of central Transcaucasia: thermal modelling, seismic interpretation, and low-temperature thermochronology of the eastern Adjara-Trialeti and western Kura sedimentary basins (Georgia). J. Asian Earth Sci. 237, 105355. https://doi.org/10.1016/j.jseaes.2022.105355.
- Hackley, P.C., 2020. Vitrinite reflectance analysis. In: Sorkhabi, R. (Ed.), Encyclopedia of Petroleum Geoscience, Encyclopedia of Earth Sciences Series. Springer

International Publishing, Cham, pp. 1–14. https://doi.org/10.1007/978-3-319-02330-4 85-1

- Hsu, C.S., Robinson, P.R. (Eds.), 2017. Springer Handbook of Petroleum Technology. Springer Handbooks. Springer International Publishing, Cham. https://doi.org/10.1007/978-3-319-49347-3
- Hu, J., Ma, Y., Li, Z., Wu, Y., Gao, W., Peng, B., Wei, X., Liu, D., 2020a. Jurassic sediments geochemical constraints on provenance, weathering process, and palaeoclimate variation of the north margin of Qaidam Basin, north-eastern Tibetan Plateau. Geol. J. 55 (4), 3247–3257. https://doi.org/10.1002/gi.3542.
- Hu, J., Tang, Y., He, D., Bo, N., Li, M., 2020b. Comparison and exploration of hydrocarbon expulsion patterns of different types of source rocks. J. Geomechanics 26 (6), 941–951 j.issn.1006-6616.2020.26.06.075 (in Chinese).
- Jiang, S., Zuo, Y., Yang, M., Feng, R., 2021. Reconstruction of the Cenozoic tectonothermal history of the Dongpu Depression, Bohai Bay Basin, China: constraints from apatite fission track and vitrinite reflectance data. J. Petrol. Sci. Eng. 205, 108809. https://doi.org/10.1016/j.petrol.2021.108809.
- Jiao, D., Liu, C., Liu, W., Su, H., He, J., Zhao, Z., Ye, B., Xu, X., 2020. Petrogenesis and tectonic significance of the late Devonian-early Carboniferous Jianxiashan pluton in the western domain of the eastern Kunlun Orogen, northern Tibetan Plateau. Geol. J. 55 (9), 6198–6215. https://doi.org/10.1002/gj.3804.
- Ketcham, R.A., 2005. Forward and inverse modeling of low-temperature thermochronometry data. Rev. Mineral. Geochem. 58, 275–314. https://doi.org/10.2138/rmg.2005.58.11.
- Ketcham, R.A., Carter, A., Donelick, R.A., Barbarand, J., Hurford, A.J., 2007. Improved modeling of fission-track annealing in apatite. Am. Mineral. 92, 799–810. https://doi.org/10.2138/am.2007.2281.
- Kuang, L., Hou, L., Wu, S., Cui, J., Tian, H., Zhang, L., Zhao, Z., Luo, X., Jiang, X., 2022. Organic matter occurrence and pore-forming mechanisms in lacustrine shales in China. Petrol. Sci. 19 (4), 1460–1472. https://doi.org/10.1016/ j.petsci.2022.03.005.
- Landry, K.R., Coutand, I., Whipp, Jr.D.M., Grujic, D., Hourigan, J.K., 2016. Late Neogene tectonically driven crustal exhumation of the Sikkim Himalaya: insights from inversion of multithermochronologic data. Tectonics 35 (3), 833–859. https://doi.org/10.1002/2015TC004102.
- Li, J., 2006. Permian geodynamic setting of Northeast China and adjacent regions: closure of the Paleo-Asian Ocean and subduction of the Paleo-Pacific Plate. J. Asian Earth Sci. 26 (3), 207–224. https://doi.org/10.1016/j.jseaes.2005.09.001.
- Li, R., Pei, X., Li, Z., Pei, L., Chen, G., Liu, Z., Chen, Y., Liu, C., Wang, M., Zhang, M., 2022. Paleo-tethyan ocean evolution and indosinian orogenesis in the East Kunlun orogen, northern Tibetan plateau. Minerals 12 (12), 1590. https://doi.org/10.3390/min12121590.
- Liu, C., Ma, Y., Zhou, G., Yin, C., Du, J., Gong, W., 2012. Evidence for the carboniferous hydrocarbon generation in Qaidam Basin. Acta Pet. Sin. 33 (6), 925–931. https:// doi.org/10.7623/syxb201206002 (in Chinese).
- Liu, C., Zhang, Y., Yang, S., Li, Z., Tian, J., Peng, B., Ma, Y., Yang, Y., Kong, H., 2020a. Marine frontier basin petroleum resources assessment: a case study of the Carboniferous of the Delingha depression, Qaidam Basin. Earth Sci. Front. 28 (1), 295–307. https://doi.org/10.13745/j.esf.sf.2020.5.27 (in Chinese).
- Liu, J., Qian, T., 2023. Discovery of Permian tuff from the northern margin of the Qaidam Basin and its geological implications. J. Geomechanics 29 (2), 290–300, 90/j.issn.1006-6616.2023002 (in Chinese).
- Liu, K., Li, Z., Shi, X., Wei, X., Ren, Z., Yang, X., Peng, B., 2020b. Late Hercynian-Indosinian denudation and uplift history in the eastern Qaidam Basin: constraints from multiple thermometric indicators and sedimentary evidences. Chin. J. Geophys. 63 (4), 1403–1421. https://doi.org/10.6038/cjg2020M0566 (in Chinese).
- Liu, Y., Genser, J., Neubauer, F., Jin, W., Ge, X., Handler, R., Takasu, A., 2005. 40Ar/ 39Ar mineral ages from basement rocks in the Eastern Kunlun Mountains, NW China, and their tectonic implications. Tectonophysics 398 (3), 199–224. https://doi.org/10.1016/j.tecto.2005.02.007.
- Liu, Y., Yang, S., Hu, K., Cao, J., Bian, L., Wang, L., Wang, L., 2007. Organic geochemical characteristics and hydrocarbon generation potential of source rocks in the 7th member of Dameigou Formation, Middle Jurassic, north margin of Qaidam Basin. Geol. J. China Univ. 13 (4), 703–713, 1006-7493(2007)04-0703-11 (in Chinese).
- Li, Z., Gao, J., Zheng, Z., Liu, C., Ma, Y., Zhao, Y., 2015. Present day heat flow and tectonic thermal evolution since the late Paleozoic time of the Qaidam Basin. Chin. J. Geophys. 58 (10), 3687–3705. https://doi.org/10.6038/cjg2015021 (in Chinese).
- Li, Z., Peng, B., Ma, Y., Hu, J., Wei, X., Ma, L., Fang, X., Yang, Y., Liu, K., 2019. Progress of carboniferous oil and gas survey in Qaidam Basin. Geol. Surv. China. 6 (4), 79–87, 2095-8706(2019)04-0079-09 (in Chinese).
- Li, Z., Qiu, N., Ma, Y., Guo, Y., Xiao, Y., Zhao, W., 2017. The tectono-thermal evolution in the eastern Qaidam Basin since the Paleozoic, NW China. Earth Sci. Front. 24 (3), 157–167. https://doi.org/10.13745/j.esf.2017.03.014 (in Chinese).
- Mackintosh, V., Kohn, B., Gleadow, A., Tian, Y., 2017. Phanerozoic morphotectonic evolution of the Zimbabwe Craton: unexpected outcomes from a multiple lowtemperature thermochronology study. Tectonics 36 (10), 2044–2067. https:// doi.org/10.1002/2017TC004703.
- Ma, L., Jiang, W., Xiao, Z., Li, Z., Peng, B., Hu, J., Dong, M., 2020. Discussion on the age attribution of the zabusagaxiu formation in the eastern Qaidam Basin. J. Geomechanics 26 (6), 961–972. https://doi.org/10.12090/j.issn.1006-6616.2020.26.06.077 (in Chinese).
- Mao, L., Wang, L., Zhang, J., Fu, S., Xiao, A., Liang, X., 2020. Mid-miocene initiation of the aimunike-oulongbuluke range in the NE Qaidam Basin, implications for the

growth of the Tibetan plateau. Int. Geol. Rev. 62 (16), 2039–2052. https://doi.org/10.1080/00206814.2019.1683768.

- Ma, Y., Yin, C., Liu, C., Du, J., Cheng, H., Fan, T., 2012. The progress of Carboniferous oil and gas investigation and assessment in Qaidam Basin. Acta Geosci. Sin. 32 (2), 135–144. https://doi.org/10.3975/cagsb.2012.02.02 (in Chinese).
- Metcalfe, I., 2013. Gondwana dispersion and Asian accretion: tectonic and palaeogeographic evolution of eastern Tethys. J. Asian Earth Sci. 66, 1–33. https:// doi.org/10.1016/j.jseaes.2012.12.020.
- Meng, Q., Fang, X., 2008. Cenozoic tectonic development of the Qaidam Basin in the northeastern Tibetan plateau. In: Burchfiel, B.C., Wang, E. (Eds.), Investigations into the Tectonics of the Tibetan Plateau. Geological Society of America. https://doi.org/10.1130/2008.2444(01.
- Menold, C., 2006. Tectonic and Metamorphic Evolution of the North Qaidam Ultrahigh-Pressure Metamorphic Terrane, Western China. University of California. Ph.D. dissertation.
- Meyer, B., Tapponnier, P., Bourjot, L., Métivier, F., Gaudemer, Y., Peltzer, G., Shunmin, G., Zhitai, C., 1998. Crustal thickening in Gansu-Qinghai, lithospheric mantle subduction, and oblique, strike-slip controlled growth of the Tibet plateau. Geophys. J. Int. 135 (1), 1–47. https://doi.org/10.1046/j.1365-246X.1998.00567.x.
- Pan, G., Wang, L., Li, R., Yuan, S., Ji, W., Yin, F., Zhang, W., Wang, B., 2012. Tectonic evolution of the qinghai-tibet plateau. J. Asian Earth Sci. 53, 3—14. https://doi.org/10.1016/j.jseaes.2011.12.018.
- Pang, B., Chen, J., Pang, X., Hu, T., Sheng, Y., 2024. Driving forces and their relative contributions to hydrocarbon expulsion from deep source rocks: a case of the Cambrian source rocks in the Tarim Basin. Petrol. Sci. 20 (1), 20–33. https://doi.org/10.1016/j.petsci.2022.08.011.
- Pang, J., Yu, J., Zheng, D., Wang, W., Ma, Y., Wang, Y.Z., Li, C., Li, Y., Wang, Y., 2019. Neogene expansion of the qilian Shan, north Tibet: implications for the dynamic evolution of the Tibetan plateau. Tectonics 38 (3), 1018–1032. https://doi.org/10.1029/2018TC005258.
- Peng, B., Liu, C., Qi, K., Liu, D., Wang, J., Li, Z., Ma, Y., Hu, J., 2021. Sedimentary differentiation characteristics of and the main factors controlling the Upper Devonian -Lower Carboniferous sediments in the eastern Qaidam Basin. Earth Sci. Front. 28 (1), 104–114. https://doi.org/10.13745/j.esf.sf.2020.5.11 (in Chinese).
- Peng, Y., 2015. The Late Hercynian-Indosinian Structural Characteristics of the Zongwulong Tectonic Belt in North Qaidam Basin. Ph.D. dissertation, Chinese Academy of Geological Sciences, Beijing (in Chinese).
- Qinghai Bureau of Geology and Mineral Resources (QBGMR), 1978. Regional Geological Investigation of the Delingha Area. Geological Publishing House, Beijing (in Chinese).
- Qinghai Bureau of Geology and Mineral Resources (QBGMR), 1991. Reoginal Geology of Qinghai Province. Geological Publishing House, Beijing (in Chinese).
- Qiu, N., Chang, J., Zhu, C., Liu, W., Zuo, Y., Xu, W., Li, D., 2022. Thermal regime of sedimentary basins in the Tarim, upper yangtze and north China cratons, China. Earth Sci. Rev. 224, 103884. https://doi.org/10.1016/j.earscirev.2021.103884.
- Qiu, N., Jiang, G., Mei, Q., Chang, J., Wang, S., Wang, J., 2011. The Paleozoic tectonothermal evolution of the Bachu Uplift of the Tarim Basin, NW China: constraints from (U–Th)/He ages, apatite fission track and vitrinite reflectance data. J. Asian Earth Sci. 41 (6), 551–563. https://doi.org/10.1016/j.jseaes.2011.02.008.
- Qiu, N., Zuo, Y., Chang, J., Li, W., 2014. Geothermal evidence of meso-cenozoic lithosphere thinning in the jiyang sub-basin, bohai bay basin, eastern north China craton. Gondwana Res. 26 (3), 1079–1092. https://doi.org/10.1016/i.gr.2013.08.011.
- Quinlan, G., Walsh, J., Skogseid, J., Sassi, W., Cloetingh, S., Lobkovsky, L., Bois, C., Stel, H., Banda, E., 1993. Relationship between deeper lithospheric processes and near-surface tectonics of sedimentary basins. Tectonophysics 22 (1), 217–225. https://doi.org/10.1016/0040-1951(93)90119-5.
- Reiners, P.W., Zhou, Z., Ehlers, T.A., Xu, C., Brandon, M.T., Donelick, R.A., Nicolescu, S., 2003. Post-orogenic evolution of the Dabie Shan, eastern China, from (U-Th)/He and fission-track thermochronology. Am. J. Sci. 303 (6), 489–518. https://doi.org/10.2475/ajs.303.6.489.
- Rohrmann, A., Kapp, P., Carrapa, B., Reiners, P.W., Guynn, J., Ding, L., Heizler, M., 2012. Thermochronologic evidence for plateau formation in central Tibet by 45 Ma. Geology 40 (2), 187–190. https://doi.org/10.1130/G32530.1.
- Shi, H., Li, Z., Yang, Y., Peng, B., Hu, J., Fang, X., Zhang, H., Wei, X., 2022. The factors influencing the enrichment of organic matters in the Carboniferous source rocks, Ounan depression, eastern Qaidam basin. J. Geomechanics 28 (2), 203–216. https://doi.org/10.12090/j.issn.1006-6616.2021135 (in Chinese).
- Shi, H., Hu, J., Yang, Y., Li, Z., Zhang, H., Fang, X., 2023a. Hydrocarbon generation characteristics of the Upper Carboniferous marine-continental transition source rocks in the eastern Qaidam Basin: evidences from natural gas geochemistry. Nat. Gas. Ind. 43 (11), 72–82. https://doi.org/10.3787/j.issn.1000-0976.2023.11.007 (in Chinese).
- Shi, H., Li, Z., Peng, B., Sun, Y., Zhang, H., Yang, Y., Hu, J., Fang, X., Wei, X., 2023b. The organic matter composition and hydrocarbon generation characteristics of the marine-continental transitional source rocks in the Upper Carboniferous Keluke Formation, Ounan depression, Qaidam Basin. Acta Geol. Sin. 97 (1), 179–196. https://doi.org/10.19762/j.cnki.dizhixuebao.2022231 (in Chinese).
- Song, S., Yang, L., Zhang, Y., Niu, Y., Wang, C., Su, L., Gao, Y., 2017. Qi-Qin Accretionary Belt in Central China Orogen: accretion by trench jam of oceanic plateau and formation of intra-oceanic arc in the Early Paleozoic Qin-Qi-Kun Ocean. Sci. Bull. 62 (15), 1035–1038. https://doi.org/10.1016/j.scib.2017.07.009.
- Sun, J., Chen, S., Liu, C., Ma, Y., Yin, C., 2016. Tectonic setting of northeastern Qaidam

Basin and its evolution during the Late Paleozoic: evidence from geochemical characteristics of detrital rock. Earth Sci. Front. 23 (5), 45–55. https://doi.org/10.13745/j.esf.2016.05.005 (in Chinese).

- Sun, J., Dong, Y., Ma, L., Chen, S., Jiang, W., 2022. Devonian to Triassic tectonic evolution and basin transition in the East Kunlun—Qaidam area, northern Tibetan Plateau: constraints from stratigraphy and detrital zircon U—Pb geochronology. Geol. Soc. Am. Bull. 134 (7–8), 1967—1993. https://doi.org/ 10.1130/B36147.1.
- Sun, J., Dong, Y., Ma, L., Peng, Y., Chen, S., Du, J., Jiang, W., 2019. Late Paleoproterozoic tectonic evolution of the Olongbuluke Terrane, northern Qaidam, China: constraints from stratigraphy and detrital zircon geochronology. Precambrian Res. 331, 105349. https://doi.org/10.1016/j.precamres.2019.105349.
- Sweeney, J.J., Burnham, A.K., 1990. Evaluation of a simple model of vitrinite reflectance based on chemical kinetics1. AAPG Bull. 74 (10), 1559–1570. https://doi.org/10.1306/0C9B251F-1710-11D7-8645000102C1865D.
- Tapponnier, P., Zhiqin, X., Roger, F., Meyer, B., Arnaud, N., Wittlinger, G., Jingsui, Y., 2001. Oblique stepwise rise and growth of the Tibet Plateau. Science 294 (5547), 1671–1677, 126/science.105978.
- Tang, X., Yang, S., Hu, S., 2023. Tectonic-thermal history and hydrocarbon potential of the Pearl River Mouth Basin, northern South China Sea: insights from borehole apatite fission-track thermochronology. China Geology 6 (3), 429–442. https://doi.org/10.31035/cg2022055.
- Tang, X., Chen, L., Hu, S., Yang, S., Zhang, G., Shen, H., Rao, S., Li, W., 2014. Tectonothermal evolution of the reed bank basin, southern south China sea. J. Asian Earth Sci. 96, 344–352. https://doi.org/10.1016/j.jseaes.2014.09.030.
  Tang, X., Zuo, Y., Kohn, B., Li, Y., Huang, S., 2019. Cenozoic thermal history recon-
- Tang, X., Zuo, Y., Kohn, B., Li, Y., Huang, S., 2019. Cenozoic thermal history reconstruction of the Dongpu Sag, Bohai Bay Basin: insights from apatite fission-track thermochronology. Terra. Nova 31 (3), 159–168. https://doi.org/10.1111/ter.12379
- Wang, F., Feng, H., Shi, W., Zhang, W., Wu, L., Yang, L., Wang, Y., Zhang, Z., Zhu, R., 2016. Relief history and denudation evolution of the northern Tibet margin: constraints from <sup>40</sup>Ar/<sup>39</sup>Ar and (U—Th)/He dating and implications for far-field effect of rising plateau. Tectonophysics 675, 196–208. https://doi.org/10.1016/j.tecto.2016.03.001.
- Wang, J., Guo, S., 2021. Study on the relationship between hydrocarbon generation and pore evolution in continental shale from the Ordos Basin, China. Petrol. Sci. 18 (5), 1305–1322. https://doi.org/10.1016/j.petsci.2021.01.002.
- Wang, J., Li, Z., Liu, K., 2022. Rehabilitation status of denuded land in the eastern Qaidam Basin: geophysical and thermochronological evidences. Earth Sci. Front. 29 (4), 371–384. https://doi.org/10.13745/j.esf.sf.2021.12.6 (in Chinese).
- Wang, J., Shi, W., Zhong, C., Hu, J., 2024. The Late Cenozoic crustal deformation in the northeastern periphery of the Qaidam Basin, northwest China. Geol. J. 59 (5), 1663–1681. https://doi.org/10.1002/gj.4958.
- Wang, L., Cheng, F., Zuza, A.V., Jolivet, M., Liu, Y., Guo, Z., Li, X., Zhang, C., 2021. Diachronous growth of the Northern Tibetan Plateau derived from flexural modeling. Geophys. Res. Lett. 48 (8), e2020GL092346. https://doi.org/10.1029/ 2020GL092346.
- Wang, L., MacLennan, S.A., Cheng, F., 2020. From a proximal-deposition-dominated basin sink to a significant sediment source to the Chinese Loess Plateau: insight from the quantitative provenance analysis on the Cenozoic sediments in the Qaidam basin, northern Tibetan Plateau. Palaeogeogr. Palaeoclimatol. Palaeoecol. 556, 109883. https://doi.org/10.1016/j.palaeo.2020.109883.
- Wei, X., Ma, Y., Li, Z., Qi, K., Guo, y., Peng, B., Hu, J., Liu, K., 2018. High frequency alternation and driving mechanisms of clastic-carbonate successions in the Upper Carboniferous, northern Qaidam Basin. Journal of Paleogeography (Chinese Edition) 20 (3), 409–422, 107605/gdlxb.2018.03.030 (in Chinese).
- Wei, X., Li, Z., Ma, Y., Li, Y., Hu, J., Liu, K., Fang, X., 2021. Sedimentology and sequence stratigraphy of the mixed clastic-carbonate deposits in the Late Paleozoic icehouse period: a case study from the northern Qaidam Basin. China Geology 4 (4), 673–685. https://doi.org/10.31035/cg2021068.
- Wu, C., Yin, A., Zuza, A.V., Zhang, J., Liu, W., Ding, L., 2016. Pre-Cenozoic geologic history of the central and northern Tibetan Plateau and the role of Wilson cycles in constructing the Tethyan orogenic system. Lithosphere 8 (3), 254–292. https://doi.org/10.1130/L494.1.
- Wygrala, B.P., 1989. Integrated study of an oil field in the southern Po basin, northern Italy. Ber. Kernforsch. Julich 2313, 1–217.
- Xia, R., Wang, C., Deng, J., Carranza, E.J.M., Li, W., Qing, M., 2014. Crustal thickening prior to 220 Ma in the East Kunlun orogenic belt: insights from the late triassic granitoids in the xiao-nuomuhong pluton. J. Asian Earth Sci. 93, 193–210. https://doi.org/10.1016/j.jseaes.2014.07.013.
- Xiao, W., Windley, B.F., Yong, Y., Yan, Z., Yuan, C., Liu, C., Li, J., 2009. Early paleozoic to devonian multiple-accretionary model for the qilian Shan, NW China. J. Asian Earth Sci. 35 (3), 323–333. https://doi.org/10.1016/j.jseaes.2008.10.001.
- Xiong, Y., Liu, B., Tan, X., Hou, Z., Luo, J., Xie, Y., Shi, K., Wu, K., 2024. Reactive transport modeling constraints on the complex genesis of a lacustrine dolomite reservoir: a case from the Eocene Qaidam Basin. Petrol. Sci. https://doi.org/10.1016/j.petsci.2024.03.008.
- Xu, W., Bao, J., Liu, T., Yin, X., 2008. Evaluation of lower jurassic source rocks in lenghu area, northern margin of Qaidam Basin. Nat. Gas Geosci. 19 (5), 707–712, 1672-1926(2008)05-0707-06 (in Chinese).
- Xu, W., Zhou, Y., Zhang, J., Li, Y., 2023. Thermo-tectonic evolution of the northern Erlian Basin (NE China): evidence from fission track and (U—Th)/He thermochronology. J. Asian Earth Sci. 248, 105620. https://doi.org/10.1016/ i.jseaes.2023.105620.
- Xu, X., Xu, S., Liu, J., Chen, L., Liang, H., Mei, L., Liu, Z., Shi, W., 2021. Thermal

maturation, hydrocarbon generation and expulsion modeling of the source rocks in the baiyun sag, pearl river mouth basin, south China sea. J. Petrol. Sci. Eng. 205, 108781. https://doi.org/10.1016/j.petrol.2021.108781.

- Yan, Z., Guo, X., Fu, C., Aitchison, J., Wang, Z., Li, J., 2014. Detrital heavy mineral constraints on the triassic tectonic evolution of the West qinling terrane, NW China: implications for understanding subduction of the paleotethyan ocean. J. Geol. 122 (5), 591–608. https://doi.org/10.1086/677264.
- Yang, M., Zuo, Y., Yan, K., Zhou, Y., Zhang, Y., Zhang, C., 2022. Hydrocarbon generation history constrained by thermal history and hydrocarbon generation kinetics: a case study of the Dongpu Depression, Bohai Bay Basin, China. Petrol. Sci. 19 (2), 472–485. https://doi.org/10.1016/j.petsci.2021.10.009.
- Yang, P., Ren, Z., Fu, J., Bao, H., Xiao, H., Shi, Z., Wang, K., Zhang, Y., Liu, W., Li, W., 2023. A tectono-thermal perspective on the petroleum generation, accumulation and preservation in the southern ordos Basin, North China. Petrol. Sci. https://doi.org/10.1016/j.petsci.2023.12.006.
- Ye, Y., Wu, L., Cowgill, E., Tian, Y., Lin, X., Xiao, A., Chen, H., 2022. Long-lagged (~19 Myr) response of accelerated river incision to rock uplift on the northern margin of the Tibetan Plateau. Earth Planet Sci. Lett. 591, 117608. https://doi.org/10.1016/j.epsl.2022.117608
- Yin, A., Dang, Y.-Q., Zhang, M., Chen, X.-H., McRivette, M.W., 2008. Cenozoic tectonic evolution of the Qaidam basin and its surrounding regions (Part 3): structural geology, sedimentation, and regional tectonic reconstruction. Geol. Soc. Am. Bull. 120 (7–8), 847–876. https://doi.org/10.1130/B26232.1.
- Yin, A., Rumelhart, P.E., Butler, R., Cowgill, E., Harrison, T.M., Foster, D.A., Ingersoll, R.V., Qing, Z., Xian-Qiang, Z., Xiao-Feng, W., Hanson, A., Raza, A., 2002. Tectonic history of the Altyn Tagh fault system in northern Tibet inferred from Cenozoic sedimentation. Geol. Soc. Am. Bull. 114 (10), 1257–1295. https://doi.org/10.1130/0016-7606(2002)114-1257:THOTAT>-2.0.CO:2.
- Yu, H., Tuo, J., Liu, L., Chen, J., Zhao, L., 2000. Geochemical characteristics and hydrocarbon generation potential evaluation of Jurassic source rocks in eastern Qaidam Basin. Acta Sedimentol. Sin. 18 (1), 132–138, 1000-0550(2000)01-0132-07 (in Chinese).
- Yu, X., Guo, Z., Zhang, Q., Cheng, X., Du, W., Wang, Z., Bian, Q., 2017. Denan Depression controlled by northeast-directed Olongbulak Thrust Zone in northeastern Qaidam basin: implications for growth of northern Tibetan Plateau. Tectonophysics 717, 116–126. https://doi.org/10.1016/ j.tecto.2017.06.017.
- Zhang, W., 2017. Thermal history and maturity evolution history from

- Carboniferous to present in eastern Qaidam Basin during the Indosinian Period. Master's Dissertation. Chengdu University of Technology (in Chinese).
- Zhao, G., Cawood, P.A., 2012. Precambrian geology of China. Precambrian Res. 222–223, 13–54. https://doi.org/10.1016/j.precamres.2012.09.017.
- Zhao, G., Wang, Y., Huang, B., Dong, Y., Li, S., Zhang, G., Yu, S., 2018. Geological reconstructions of the East asian blocks: from the breakup of rodinia to the assembly of Pangea. Earth Sci. Rev. 186, 262–286. https://doi.org/10.1016/j.earscirev.2018.10.003.
- Zheng, D., Pang, X., Ma, X., Li, C., Zheng, T., Zhou, L., 2019. Hydrocarbon generation and expulsion characteristics of the source rocks in the third member of the Upper Triassic Xujiahe Formation and its effect on conventional and unconventional hydrocarbon resource potential in the Sichuan Basin. Mar. Petrol. Geol. 109, 175–192. https://doi.org/10.1016/j.marpetgeo.2019.06.014.
- Zhong, C., Tang, X., Wang, J., 2024a. How did the late Paleozoic to early Mesozoic tectonism constrain the Carboniferous stratigraphic evolution in the eastern Qaidam Basin, NW China? Geosci 14 (2), 31. https://doi.org/10.3390/geosciences14020031.
- Zhong, C., Wu, Z., Hu, J., Li, Z., Ma, L., Wang, J., 2024b. Discovery of the Lower Permian strata from the west section of the northern margin of the Qaidam Basin and its geological implications. Nat. Gas Geosci. 35 (2), 288–299. https://doi.org/10.11764/j.issn.1672-1926.2023.07.003 (in Chinese).
- Zhou, L., Li, Y., Jin, F., Xie, J., Pu, X., Fu, L., Lou, D., Tian, Y., 2023. Decipher hydrocarbon generation and accumulation based on fluid inclusion and chronology: a case study from the Upper Paleozoic buried-hills in Huanghua Depression, Bohai Bay Basin. Petrol. Sci. 20 (4), 1998–2008. https://doi.org/10.1016/j.petsci.2023.03.010.
- Zhu, C., Hu, S., Qiu, N., Jiang, Q., Rao, S., Liu, S., 2018. Geothermal constraints on Emeishan mantle plume magmatism: paleotemperature reconstruction of the Sichuan Basin, SW China. Int. J. Earth Sci. 107 (1), 71–88. https://doi.org/10.1007/s00531-016-1404-2.
- Zuza, A.V., Wu, C., Reith, R.C., Yin, A., Li, J., Zhang, J., Zhang, Y., Wu, L., Liu, W., 2017. Tectonic evolution of the Qilian Shan: an early Paleozoic orogen reactivated in the Cenozoic. Geol. Soc. Am. Bull. 130 (5–6), 881–925. https://doi.org/10.1130/ B31721.1.
- Zuza, A.V., Yin, A., 2017. Balkatach hypothesis: a new model for the evolution of the Pacific, Tethyan, and Paleo-Asian oceanic domains. Geosphere 13 (3), 1664–1712. https://doi.org/10.1130/GES01463.1.